EUROPEAN COMMISSION

Community Research

SEVENTH FRAMEWORK PROGRAMME

CARBOWASTE

Treatment and Disposal of Irradiated Graphite and Other Carbonaceous Waste

Grant Agreement Number: FP7-211333

Technical Report T-3.4.2

Assessment of Isotope-Accumulation Data from RBMK-1500 Reactor

Author(s):

Ernestas Norkūnas, Artūras Šmaižys, Povilas Poškas

Lithuanian Energy Institute

Rūta Druteikienė, Grigorijus Duškesas, Andrius Garbaras, Arūnas Gudelis, Rasa Gvozdaitė, Galina Lujanienė, Rita Plukienė, Artūras Plukis, Andrius Puzas

Fizinių ir technologijos mokslų centras

Document Number: CARBOWASTE-T-1105-3.4.2

Date of issue of this report: 24/05/2013

Project co-funded by the European Commission under the Seventh Framework Programme (2007 to 2012) of the European Atomic Energy Community (EURATOM) for nuclear research and training activities		
Dissemination Level		
PU	Public	
RE	Restricted to the partners of the CARBOWASTE project	
CO	Confidential, only for specific distribution list defined on this document	**X**

Start date of project: **01/04/2008** Duration: **60 Months**

Distribution list

Person and organisation name and/or group	Comments
Task 3.4 members	
WP3 members	
WP4 members	
WP5 members	
WP6 members	
Executive Board	
Co-ordinator	

CARBOWASTE		
Work package: 3 **Task:** 3.4	**CARBOWASTE document no:** CARBOWASTE-1105-T-3.4.2	**Document type:** Technical Report
Issued by: Fizinių ir technologijos mokslų centras (LT) **Internal no.:** 203-T09_Technical_Report_3.4.2-D		**Document status:** Final

Document title

Assessment of Isotope-Accumulation Data from RBMK-1500 Reactor

Executive summary

The simulation of irradiation of RBMK-1500 reactor graphite has been performed to estimate specific activity of ^{14}C and other important for safety alpha and beta emitters in the reactor graphite stack and sleeves. Concentration of important impurities in virgin RBMK-1500 reactor graphite have been measured by inductively coupled plasma mass spectrometry and verified by comparison with available neutron activation data. Analysis of initial data uncertainties has been done. The created computer model for simulation of neutron activation of carbon and impurities in the RBMK-1500 reactor graphite has been validated by isotope ratio mass spectrometry, alpha and beta spectrometric measurements. For the conservative modelling case, the specific activity of the graphite blocks is in the order 10^8 Bq/g of magnitude just after the reactor final shutdown (RFS) and is higher than that of the graphite rings/sleeves (less than 10^7 Bq/g) and stays higher during all analysed cooling time. For the non-conservative case, specific activity of graphite blocks is several times lower than for conservative case, while specific activity of graphite rings/sleeves for both cases differs not significant (except ~10 years after RFS).The radionuclides ^3H, ^{55}Fe, ^{60}Co (short-lived) and ^{14}C, ^{36}Cl, ^{63}Ni (long-lived) have the highest activities in the graphite constructions. Values of actinide concentration exceed unconditional clearance levels and can create an additional problem for irradiated RBMK-1500 reactor graphite waste management.

The results that come out from this task are necessary for implementation of Work Packages 4, 5, and 6.

Revisions

Rev.	Date	Short description	Author	Review	Task Leader	WP Leader
01	24/05/2013	Final report	G. Duškesas FTMC	A. Plukis FTMC	D. Vulpius FZJ	G. Pina Lukas CIEMAT

Table of Content

GLOSSARY 6

1 INTRODUCTION 7

2 NEUTRON ACTIVATION ASSESSMENT METHODOLOGY 8

2.1 Modelling of spatial and energetic distribution of neutron flux 10

2.2 Modelling of the neutron activation of the materials 15

2.3 Influence of uncertainty of cross sections of carbon isotopes for evaluation of the neutron fluence in the graphite 17

2.4 Evaluation method to restore the irradiation parameters of graphite 18
2.4.1 Modelling of activation of carbon isotopes in the graphite constructions 19
2.4.2 Sampling and experimental equipment 21
2.4.3 Evaluation of the integral neutron flux 24

3 INITIAL MATERIAL COMPOSITION 27

3.1 Determination of impurities of the reactor graphite by mass spectrometric technique 28
3.1.1 Preparation of samples 28
3.1.2 Instruments 28
3.1.3 Results 30

3.2 Comparison of available data on impurities in RBMK-1500 reactor virgin graphite 33

4 SPATIAL AND ENERGETIC NEUTRON FLUX DISTRIBUTION 37

4.1 Graphite blocks 37

4.2 Graphite rings/sleeves 38

4.3 FCs central parts 39

4.4 Discussion 40

5 INFLUENCE OF UNCERTAINTY OF CONCENTRATION OF IMPURITIES ON NEUTRON ACTIVATION MODELLING 46

5.1 Graphite rings/sleeves 46
5.1.1 Case A 46
5.1.2 Case B 47
5.1.3 Comparison of the results 49

5.2 Graphite blocks 50
5.2.1 Case A 50

5.2.2 Case B 52
5.2.3 Comparison of the results 55

5.3 Discussion 56

6 INFLUENCE OF NITROGEN ACTIVATION ON ^{14}C CONCENTRATION 57

7 INFLUENCE OF RADIONUCLIDE ACTIVITY ON MANAGEMENT OF GRAPHITE IRRADIATED IN RBMK-1500 REACTOR 59

8 VALIDATION OF ACTIVITY CALCULATION MODEL 61

9 SUMMARY AND CONCLUSIONS 63

10 REFERENCES 65

Glossary

AAS	Atom Absorption Spectrometer
FC	Fuel Channel
ICP-MS	Inductively Coupled Plasma Mass Spectrometry
IRMS	Isotope Ratio Mass Spectrometry
LSC	Liquid Scintillation Counting
NPP	Nuclear Power Plant
RFS	Reactor final Shutdown

1 Introduction

There is one Nuclear Power Plant (Ignalina NPP) in Lithuania, which consists of two Units with RBMK-1500 water-cooled graphite-moderated channel-type power reactors. Unit 1 was shut down at the end of 2004 while Unit 2 was shut down in the end of 2009.

Cross section of RBMK-1500 reactor vault is presented in Fig. 1 [1].

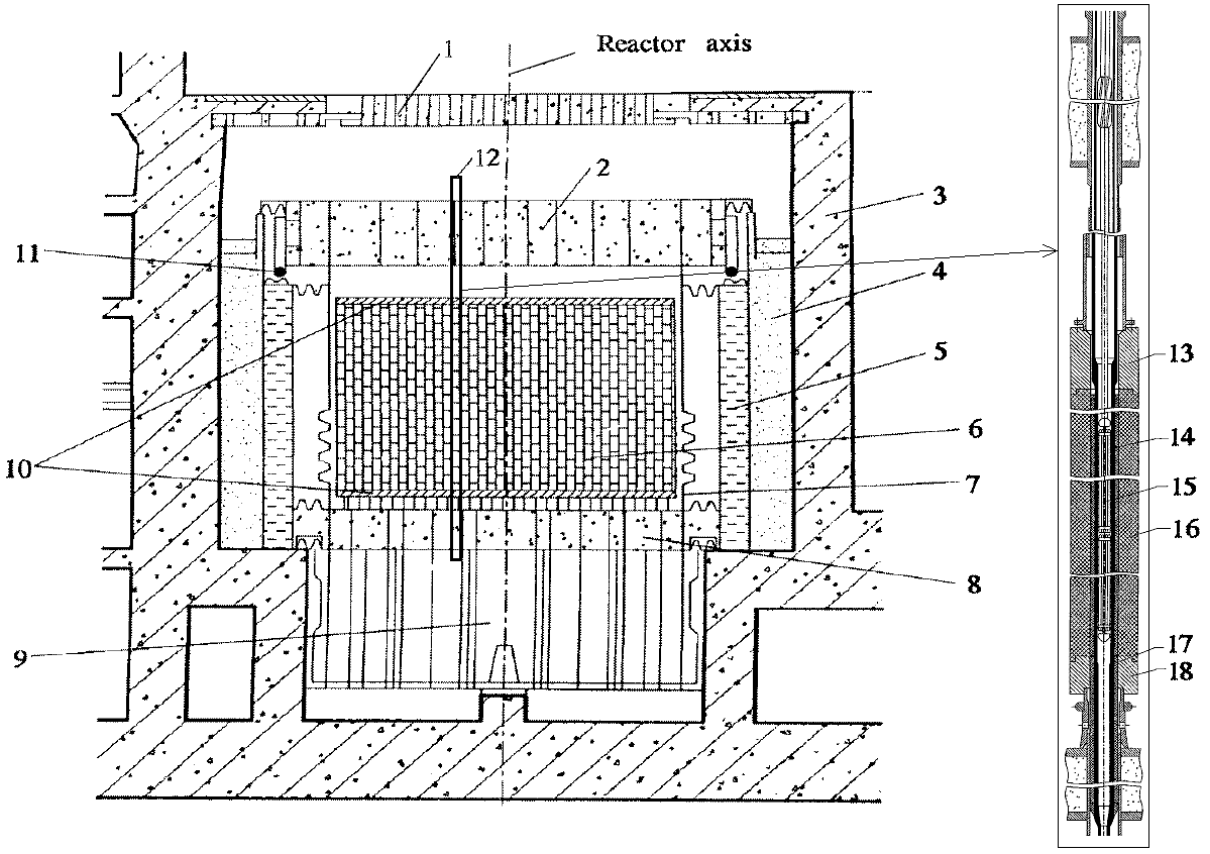

Fig. 1. Cross–section of RBMK–1500 reactor vault [1]

1 – top cover (floor of the central hall);
2 – top metal structure (with serpentinite);
3 – concrete vault;
4 – sand cylinder;
5 – water tank;
6 – graphite stack;
7 – reactor shell;
8 – bottom metal structure (with serpentinite);
9 – reactor support structure;
10 – steel shield and support plates;
11 – roller supports;
12 – modelled segment;
13 – shield plate;
14 – FC central part;
15 – FA inside FC;
16 – graphite blocks;
17 – graphite rings/sleeves;
18 – support plate

The graphite stack (6) serves as a neutron moderator and reflector. The graphite stack consist of individual graphite blocks (16) made of GR-280 grade graphite and can be visualized as a

vertical cylinder, made up of 2488 graphite columns (8 m height), constructed from different types of graphite blocks. The upper and the lower 0.5 m thick graphite stack layers are called respectively top and bottom reflectors as there is no fuel in these regions and graphite is mainly used here for neutron reflection back to the active core. The blocks are rectangular parallelepipeds, with a base of 0.25 × 0.25 m, and heights of 0.2, 0.3 and 0.6 m. The blocks have a 0.114 m diameter bore openings through the vertical axis, and this provides a total of 2044 fuel (technological) channels (14) which are used for placing fuel assemblies (15), control rods and other equipment into the core. The openings in the remaining 444 peripheral graphite columns are filled with graphite rods in order to increase neutron reflection and these columns serve as radial reflector. In order to improve heat transfer from the graphite stack, the central segment of the fuel channel is surrounded by the 0.02 m high and 0.0115 m thick split GRP-2-125 grade graphite rings (17). These rings are arranged next to one another in such a manner that one is in contact with the channel, and the other with the graphite stack block. Above and below graphite rings there are also placed GRP-2-125 grade graphite sleeves of different shape compared to the rings. The graphite stack, including its hermetically sealed cavity, is called the sealed reactor space. This space is filled with a circulating helium-nitrogen mixture at an excess pressure of 0.49–1.96 kPa.

During reactor operation graphite blocks and rings/sleeves are under intensive neutron irradiation and became activated. The numerical assessment of neutron activation of these graphite components is presented in this report.

2 Neutron activation assessment methodology

The assessment of the neutron induced activities requires, as a first step, knowledge of the spatial and energy distributions of the neutron flux throughout the system. The neutron flux is then used to determine the individual reaction rates of the initial radionuclides whose products give rise to the ionizing radiation. These reaction rates are then used to obtain the level of activity per unit weight of the initial element according to the reactor irradiation history and the subsequent decay time. The final stage is the calculation of the component activity from the known concentration of the initial elements in the material, from which the component is manufactured, together with the mass of the components.

A general methodology involved in the inventory calculation of activation products is summarized in Fig. 2 [2].

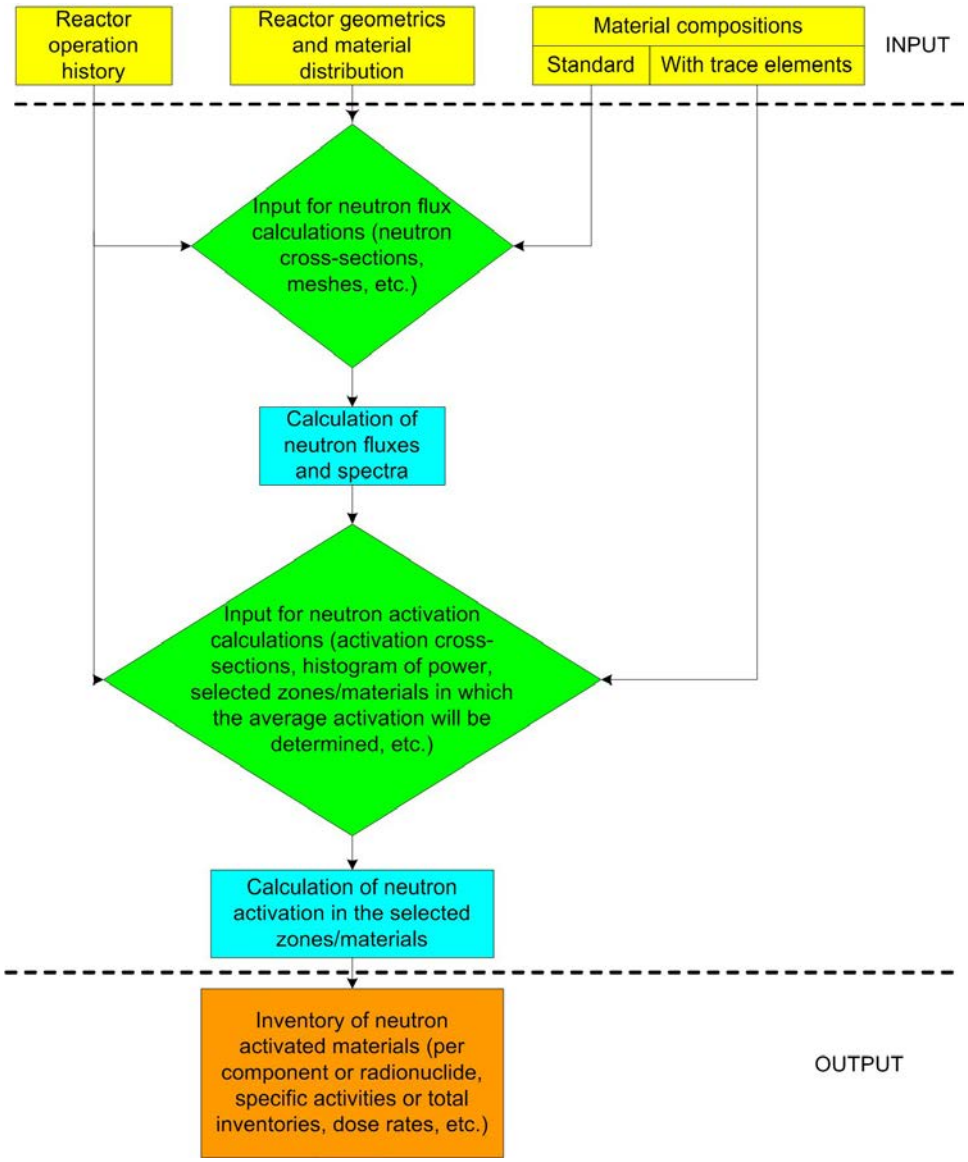

Fig. 2. General methodology for neutron induced activity calculations [2]

The inventory calculation requires the input of component averaged neutron fluxes together with specific material compositions and activation cross-sections. Numerous computer codes are available for calculating the induced activity in reactor materials. Important inputs in these calculations are the neutron energy spectrum in each region and the associated neutron flux densities [2].

2.1 Modelling of spatial and energetic distribution of neutron flux

The spatial and energy distributions of the neutron flux throughout the analysed system were obtained via numerical modelling. A general methodology used for neutron fluxes modelling in the RBMK-1500 reactor graphite structures is presented in Fig. 3. The neutron fluxes modelling requires the input of reactor operation parameters, geometrics with specific material compositions, cross-sections for neutrons transport and appropriate neutrons transport modelling code. MCNP 5 computer code (A General Purpose Monte Carlo N-Particle Transport Code) was chosen for neutron flux modelling, as this code successfully solves neutron transport problems practically in any 3D geometries and materials configuration.

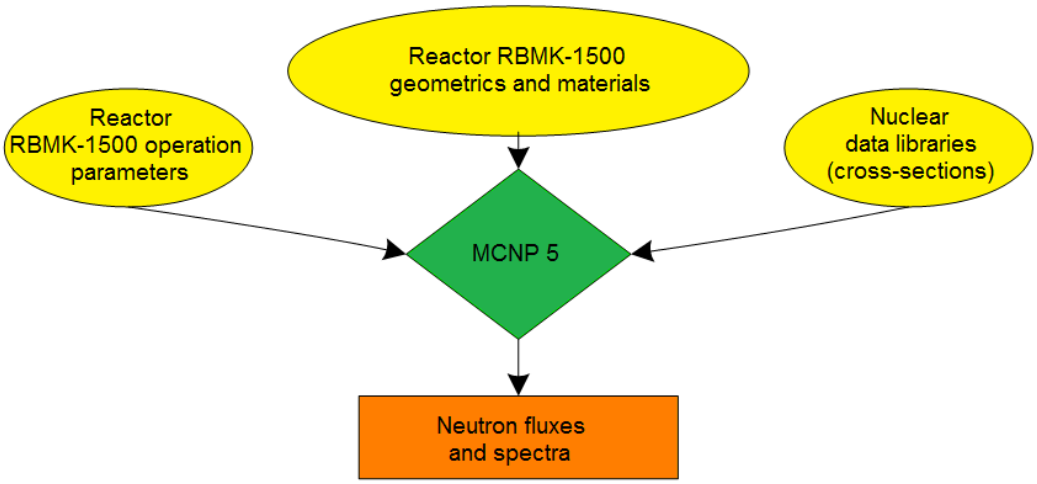

Fig. 3. A general methodology of neutron fluxes modelling

Various data of the RBMK-1500 reactor were used while developing MCNP model. These data are: geometrics of the reactor components, the materials compositions and densities, the reactor operation parameters and others. These data were based on the information presented in [1, 10]. In order to assess the impact of different fuel type (fuel with and without burnable erbium absorber) and different fuel burnup on the neutron flux distribution, 3 cases of one lattice segment model were developed in this study assuming that:

1. Fuel channel is loaded with UO_2 fuel of average burnup of ~10 MWd/kgU with 2.4 % ^{235}U enrichment and 0.41 % burnable Er_2O_3 absorber;
2. Fuel channel is loaded with fresh UO_2 fuel with 2.4 % ^{235}U enrichment and 0.41 % burnable Er_2O_3 absorber;

3. Fuel channel is loaded with fresh UO_2 fuel with 2.4 % ^{235}U enrichment.

From the beginning of its operation in 1984, Ignalina NPP Unit 1 RBMK-1500 reactor was loaded with UO_2 fuel having 2.0 % ^{235}U initial enrichment. Later, starting from 1997 UO_2 fuel with 2.4 % ^{235}U enrichment and 0.41 % burnable Er_2O_3 absorber content was introduced and from 2002 UO_2 fuel with 2.6 % ^{235}U enrichment and 0.5 % burnable Er_2O_3 absorber content was introduced. When reactor is in operation the fuel burns up and fuel assemblies with burned fuel are continuously replaced with the assemblies having fresh fuel. According to [10], the average fuel burnup in the reactor is ~11 MWd/kgU. Taking into the consideration the information on the usage of nuclear fuel with different enrichment, burnable absorber content, the information on the average fuel burnup within reactor core ant the fact, that when evaluating neutron activation of reactor components, the neutron fluxes representing average reactor operation conditions during its whole lifetime should be used, the neutron flux modelling results obtained using the first modelling case were selected to be used in the subsequent neutron activation modelling of the reactor graphite components. The radionuclide inventory of irradiated (partly spent) fuel (2.4 % ^{235}U initial enrichment and 0.41 % burnable Er_2O_3 absorber with burnup up to ~10 MWd/kgU) for this case was modelled by computer code SAS2 from SCALE 5 computer code system.

It was assumed that a fuel assembly (FA), which consists of two fuel bundles, with UO_2 fuel (2.4 % ^{235}U enrichment and 0.41 % burnable Er_2O_3 absorber) of ~10 MWd/kgU burnup is placed in a fuel channel (FC). The coolant density in the vicinity of the graphite stack is 0.5 g/cm^3 while in the bottom and top FC parts the density of the coolant was set to 0.75 g/cm^3 and 0.25 g/cm^3, respectively. The presence of spacing and intensifying grids in FA was also accounted. The temperatures of the described reactor components and other parameters were set so that they correspond to the conditions of the fuel channel working on average power (~2.61 MW) corresponding to the nominal 4200 MW reactor thermal power. A view of horizontal cross-section of one lattice segment model (25×25 cm) of the Ignalina NPP RBMK-1500 reactor, developed with MCNP 5 code, is presented in Fig. 4.

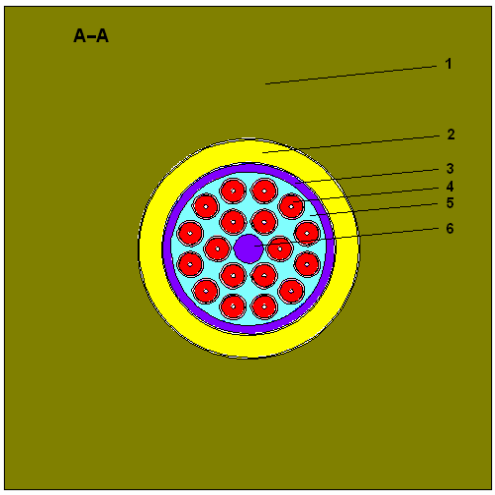

Fig. 4. Cross-section of the modelled segment of the RBMK-1500 reactor (throughout fuel bundle)

1 – graphite block;
2 – graphite ring/sleeve;
3 – FC (pressure tube);
4 – fuel element;
5 – coolant (steam–water mixture);
6 – FA central rod

The developed model itself, enveloping the graphite column with other elements inside it, the shield and support plates, the top and bottom metal structures with serpentinite fillings, etc., including the geometrical data, is given in Fig. 5.

This model of one reactor lattice cell segment, using periodic boundary conditions for the side walls of the segment, corresponds to an infinite lattice comprised of such segments and is suitable for modelling of neutron fluxes in the reactor construction elements of the central (in radial direction) core part (plateau). Suitability of such a neutron flux modelling in RBMK-1500 reactor structures is presented in [11], where it is demonstrated, that in such a manner modelled neutron fluxes in reactor fuel channels are in good agreement with results provided in reactor's safety analysis reports and etc. However, this approach is conservative because the impact of the surrounding FC with control rods in the vicinity of the analyzed segment is not accounted.

This model was also used for the evaluation of the different nuclear data libraries impact to the modelled neutron fluxes. Three data libraries (LLNL, ENDF/B-V and ENDF/B-VI) distributed with MCNP 5 code package were selected for this purpose.

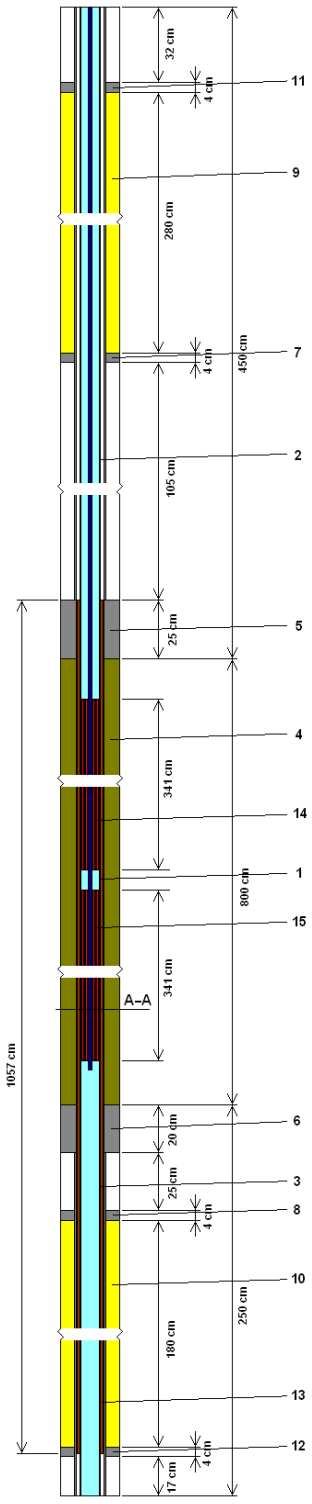

1 – FC central part;
2 – FC top part;
3 – FC bottom part;
4 – graphite blocks;
5 – steel shield plate (block);
6 – steel support plate (block);
7 – bottom steel plate of top metal structure;
8 – top steel plate of bottom metal structure;
9 – serpentinite filling of top metal structure;
10 – serpentinite filling of bottom metal structure;
11 – top steel plate of top metal structure;
12 – bottom steel plate of bottom metal structure;
13 – graphite rings/sleeves;
14 – top fuel bundle;
15 – bottom fuel bundle

Fig. 5. The analysed segment of the RBMK-1500 reactor, developed with MCNP code

In order to evaluate the impact of the position of the technological channels used for the control rods and the impact of control rods position in these channels, the second model has been developed (Fig. 6).

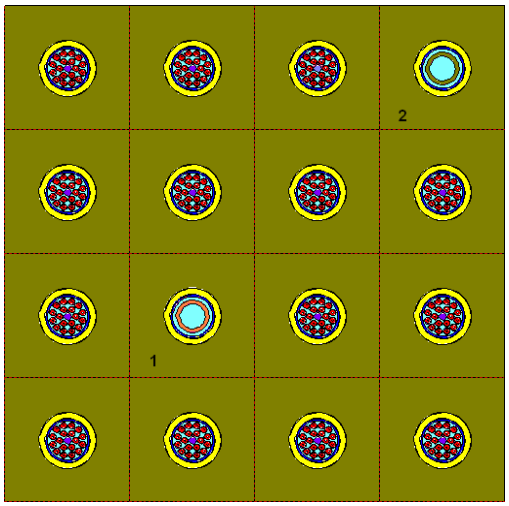

Fig. 6. Cross-section of the modelled segment (4×4 lattice cells) of the RBMK-1500 reactor

1 – cell with inserted control rod; 2 – cell with withdrawn control rod

Within this model the modelled segment of the RBMK-1500 reactor core consists of 16 cells (4x4) with two channels used for the control rods. Such a position of the fuel and technological channels with a periodic boundary conditions defined in MCNP corresponds to the real position of these channels within the central part (plateau) of the RBMK-1500 reactor [1, 10]. During the modelling it was assumed that one of the control rods is fully positioned in the technological channel and the other one is fully withdrawn. The assumptions about the fuel in the rest of channels were accepted as in the 1st case of one lattice cell model (partly spent fuel with erbium absorber).

In order to evaluate the characteristics of the neutron fluxes, their differences and variation characters, modelled reactor elements (graphite blocks and rings/sleeves, central FC part) were subdivided in to several separate zones in reactor axial direction and neutron fluxes were estimated in each of them. Modelling the neutron fluxes in this manner and analysing their axial variation characters allows properly divide these reactor constructions into different zones with different activation conditions and perform adequate evaluation of their activation.

The neutron fluxes estimated with MCNP were grouped into three energy groups:

- Thermal neutrons, with energies up to 0.625 eV;
- Resonance neutrons, with energies in range of 0.625 eV – 1 MeV;

- Fast neutrons, with energies above 1 MeV.

Such grouping of neutron fluxes was done keeping in mind, that results of this estimation are used in the second step of neutron activation modelling of reactor graphite components, i.e. induced activity modelling with ORIGEN-S computer code, which uses specifically those energy group ranges for neutron fluxes input.

2.2 Modelling of the neutron activation of the materials

A general methodology used for neutron activation modelling is presented in Fig. 7.

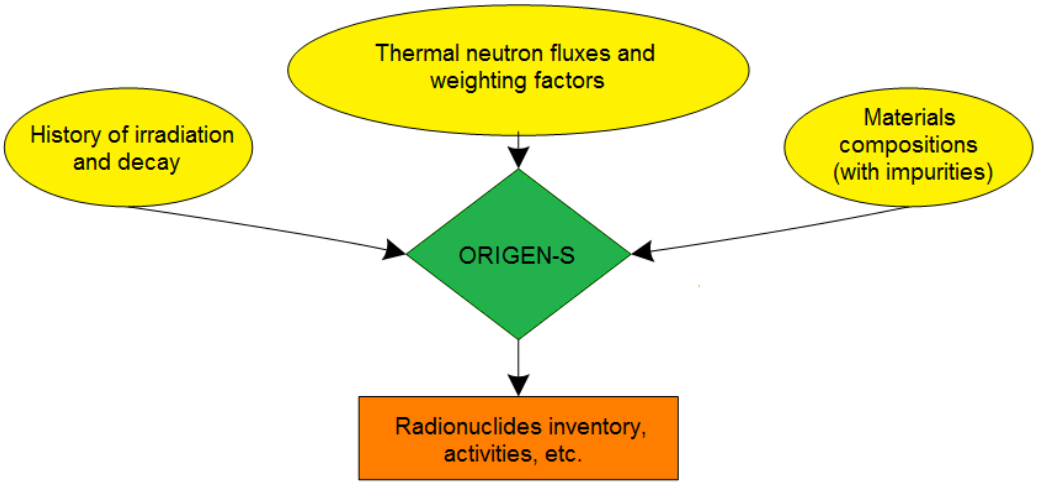

Fig. 7. A general methodology of neutron activation modelling

ORIGEN-S computer code (from SCALE 5 codes system), which is validated and verified for analysis of such processes and is widely used in the world, was used for the activation estimation. The code considers radioactive disintegration and neutron absorption (capture and fission) and enables to identify isotopic content, activities and concentrations of neutron activated materials. The time rate of the change of the concentration for a particular nuclide N_i can be written as:

$$\frac{dN_i}{dt} = \sum_j \gamma_{ji}\sigma_{f,j}N_j\phi + \sigma_{c,i-1}N_{i-1}\phi + \lambda_i^{'}N_i^{'} - \sigma_{f,i}N_i\phi - \sigma_{c,i}N_i\phi - \lambda_i N_i, \quad i = 1,\ldots I \; ; (1)$$

where

$\sum_j \gamma_{ji}\sigma_{f,j}N_j\phi$ – the yield rate of N_i due to the fission of all nuclides N_j;

$\sigma_{c,i-1}N_{i-1}\phi$ – the rate of transmutation into N_i, due to radiative neutron capture by a nuclide N_{i-1};

$\lambda_i' N_i'$ – the rate of formation of N_i due to the radioactive decay of nuclides N_i';

$\sigma_{f,i}N_i\phi$ – the destruction rate of N_i due to fission;

$\sigma_{c,i}N_i\phi$ – the destruction rate of N_i due to all forms of neutron absorption other than fission (n, γ), (n, α), (n, p), (n, $2n$) (n, $3n$);

$\lambda_i N_i$ – the radioactive decay rate of N_i.

When running ORIGEN-S as a standalone program, the input data associated with neutron fluxes are thermal neutron flux and the cross-section weighting factors THERM, RES, and FAST. Factor THERM may be determined using the moderator temperature while RES and FAST are calculated as the ratio of the resonance energy flux to the thermal flux and the ratio of the fast energy flux to the thermal flux respectively.

The real operating history of Ignalina NPP reactor Unit 1 was used for the neutron activation modelling (see Fig. 8). It was assumed that for the first 17 years (17 cycles) reactor operates at different regimes continuously without shutdowns (see Fig. 8), but during each cycle (one cycle corresponds to the one year period) operation regime remains constant. In order to evaluate activation more precisely, remaining 4 years of operation were divided into 25 shorter periods taking into account all reactor shutdowns, as presented in Fig. 8.

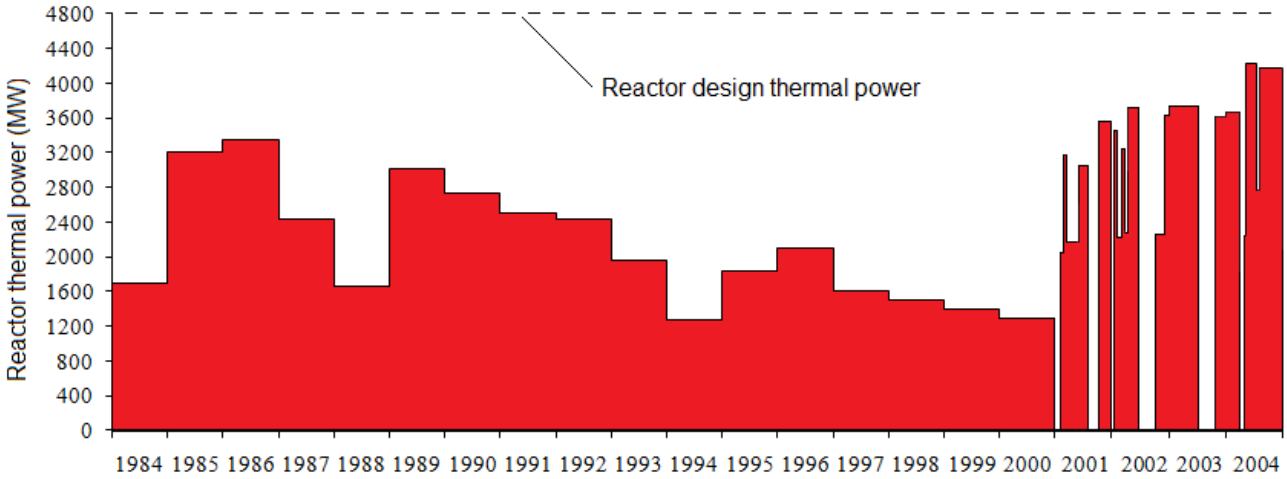

Fig. 8. The Ignalina NPP Unit 1 reactor operation history data for 1984–2004 year

As the reactor thermal power directly corresponds to the thermal neutron flux, thermal neutron fluxes for each separate cycle (used in ORIGEN-S modelling) were recalculated according to the reactor thermal power during that cycle and the neutron flux modelled for reactor operation at 4200 MW thermal power (~2.6 MW for one FC).

2.3 Influence of uncertainty of cross sections of carbon isotopes for evaluation of the neutron fluence in the graphite

As the first step of calculation, the neutron flux in the RBMK-1500 reactor graphite has been obtained by the MCNPX code (details of input are provided in [12]). An evolution of the fuel isotopic composition, activation and radioactive decay of nuclei during irradiation has been simulated with the CINDER90 code which is incorporated in MCNPX. The CINDER90 code uses 63 neutron energy groups and has its own nuclear data library composed mainly of ENDF, JEF and JENDL [13] data libraries as well as other data (e.g., for $^{13}C(n,\gamma)^{14}C$ reaction ACTL neutron activation cross section library [14] is used). The main reason why CINDER90 data library has been chosen in our work is the presence of the microscopic cross sections for $^{12}C(n,\gamma)^{13}C$ reaction in this library. These microscopic cross sections are absent in other nuclear data libraries (for instance, in JEF-3.0, JENDL-3.3 and ENDF/B-VI) where only cross section for natural C and no data for 12C isotope are present).

In [15] MCNPX code has also been used to calculate the amount of ^{14}C generated in $^{14}N(n,p)^{14}C$ reaction in a similar way considering ENDF/B-VI microscopic cross sections as in the case of $^{12}C(n, \gamma)^{13}C$, $^{13}C(n, \gamma)^{14}C$ reactions. Comparison of the newest ENDF/B-VII library nuclear data for $^{14}N(n,p)^{14}C$ reaction (which is the same as the ENDF/B-VI) with the cross section of CINDER90 shows the 2 times difference. After comparison with other sources we have decided to make correction and to use the ENDFB-VI data library cross sections for estimation of ^{14}N concentration. Microscopic cross sections for $^{14}N(n,p)^{14}C$ reaction in different data libraries are provided in Fig. 9.

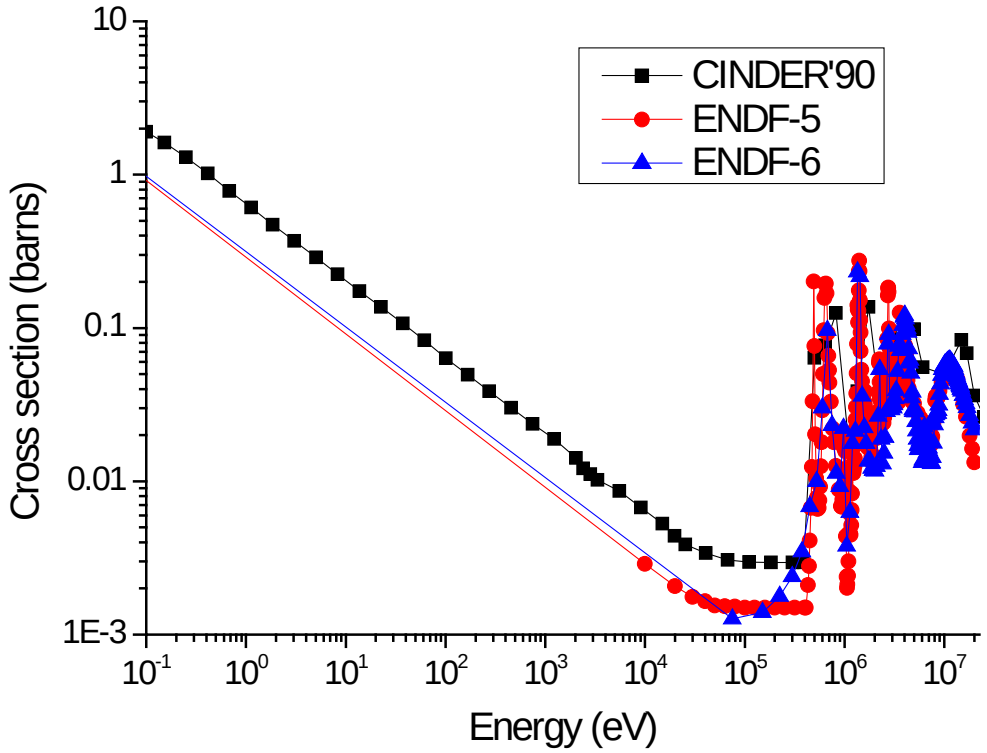

Fig. 9. Microscopic cross sections for $^{14}N(n,p)^{14}C$ reaction in different data libraries

As a result of our analysis we conclude that for precise evaluation of the neutron fluence in any position of the graphite stack or other graphite constructions in the graphite moderated reactor and for determination of ^{14}C activity in carbonaceous materials uncertainties of microscopic cross sections for reactions $^{12}C(n,\gamma)^{13}C$, $^{13}C(n,\gamma)^{14}C$, $^{13}C(n,\gamma)^{10}Be$, and $^{14}N(n,p)^{14}C$ have to be reduced.

2.4 Evaluation method to restore the irradiation parameters of graphite

In spite of the fact that the reactor power history is known, separate parts of the reactor graphite moderator undergo different conditions: changes of the neutron flux intensity and spectrum with the radial and axial position in the reactor core cause inhomogeneous activation of graphite impurities. We propose a general method, based on the results ($\delta^{13}C$ values) of mass spectrometry and the results of computer modelling of the reactor core, for evaluation of the

integral neutron flux in the graphite which can be used for calibration computer modelling to escape model input data uncertainties [12].

2.4.1 Modelling of activation of carbon isotopes in the graphite constructions

To demonstrate method capabilities we evaluated the ^{13}C and ^{14}C content of irradiated graphite of the RBMK-1500 reactor MCNPX computer code version 2.6 [16] which includes CINDER code for calculation of activation.

We have used a simplified 3D model (see in Fig. 4 horizontal section of the model) of the RBMK-1500 reactor fuel assembly in the graphite matrix. The periodical boundary conditions have been used to have more realistic Monte Carlo modelling of the reactor core. The model has been used for neutron flux calculations in the graphite sleeve and graphite stack of one fuel assembly. Furthermore, the bottom (lower part of 50 cm height) and the top (upper part of 50 cm height) reflectors of the reactor core have been investigated. The graphite and cooling water temperatures are equal to 800 K and 550 K, respectively, which correspond to the real operating conditions of the RBMK-1500 reactor. The density of the cooling water in our model is equal to 0.5 g/cm^3 and of graphite – 1.675 g/cm^3. It has been accepted that the active height of the fuel assembly is 686 cm. Also the axial distribution of power in the RBMK-1500 reactor [10] has been considered. For modelling the corrected value of the power at the active height of 375 cm of the fuel channel has been used.

In these calculations, as the first step, neutron flux in the RBMK-1500 reactor graphite has been obtained by MCNPX code. An evolution of fuel isotopic composition, activation and radioactive decay of nuclei during irradiation has been simulated with CINDER code which is incorporated in MCNPX. The CINDER code uses 63 neutron energy groups and has its own nuclear data library composed mainly of ENDF, JEF and JENDL data libraries. Nuclear data of ENDF-7 library were used in our calculations.

The neutron spectrum in the graphite does not change considerably during the fuel burn-up and depends on the graphite spatial location in the reactor (see Fig. 10 and Fig. 11 for details). This fact allows to avoid time consuming detailed calculations with CINDER code and to simplify the model using constant neutron flux (i.e. constant macroscopic cross-sections) during fuel burn-up, but variable neutron flux (i.e. variable macroscopic cross-sections) in particular graphite constructions (graphite sleeve, graphite stack, upper part of the graphite stack, etc.).

In these calculations the UO_2 fuel enriched to 2.6 % of ^{235}U and to 0.5% of burnable erbium poison has been modelled. The neutron flux and the macroscopic cross sections of nuclear reactions have been calculated for averaged burn-up of the fuel in the RBMK-1500 reactor in the particular graphite constructions. The constant fuel assembly power of 2.53 MW (which corresponds to 4200 MW full reactor power) has been used during all irradiation time. The activity of the carbon isotopes in the particular constructions of irradiated graphite has been simulated using macroscopic cross-sections of the $^{12}C(n,\gamma)^{13}C$, $^{13}C(n,\gamma)^{14}C$ reactions.

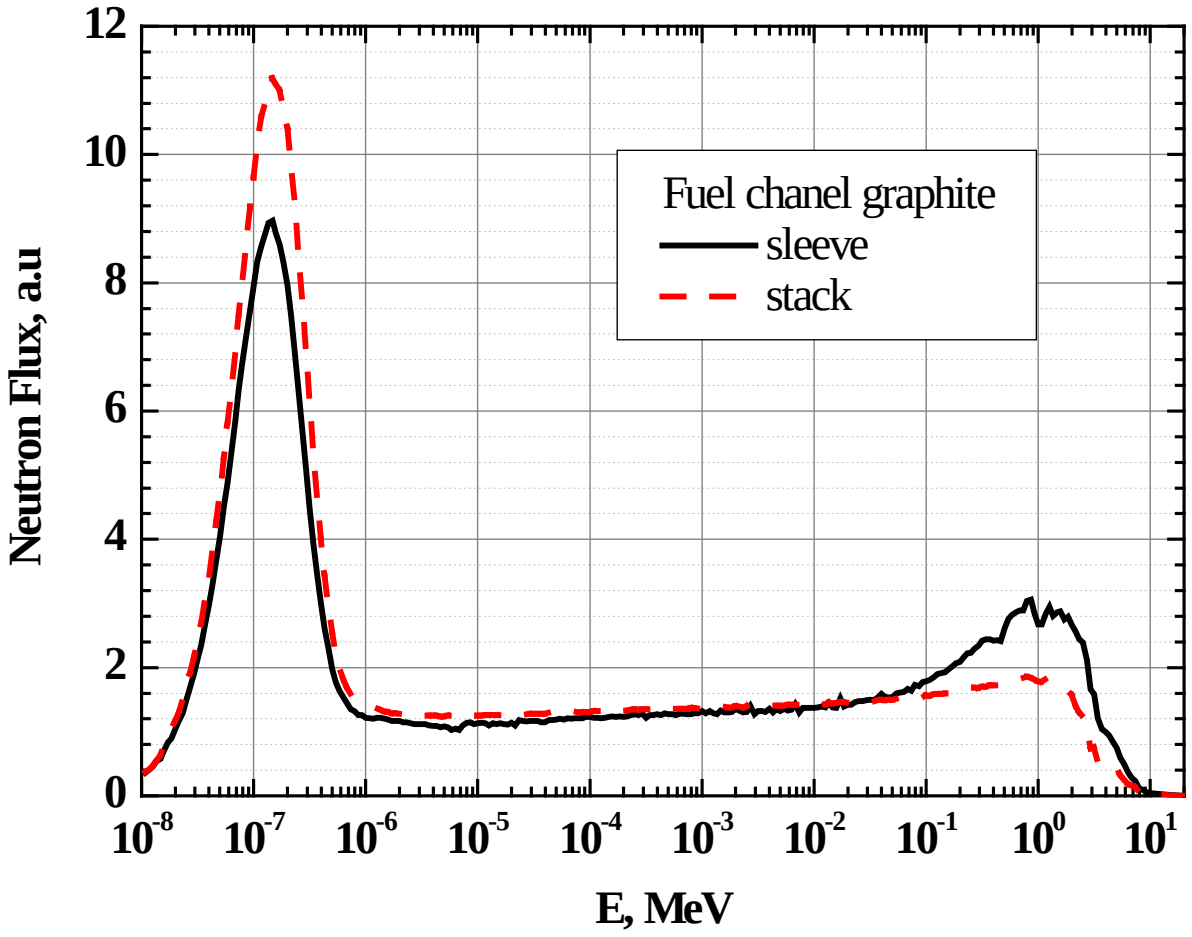

Fig. 10. Neutron energy spectrum in the graphite stack of the fuel channel and the graphite sleeve for average burn-up

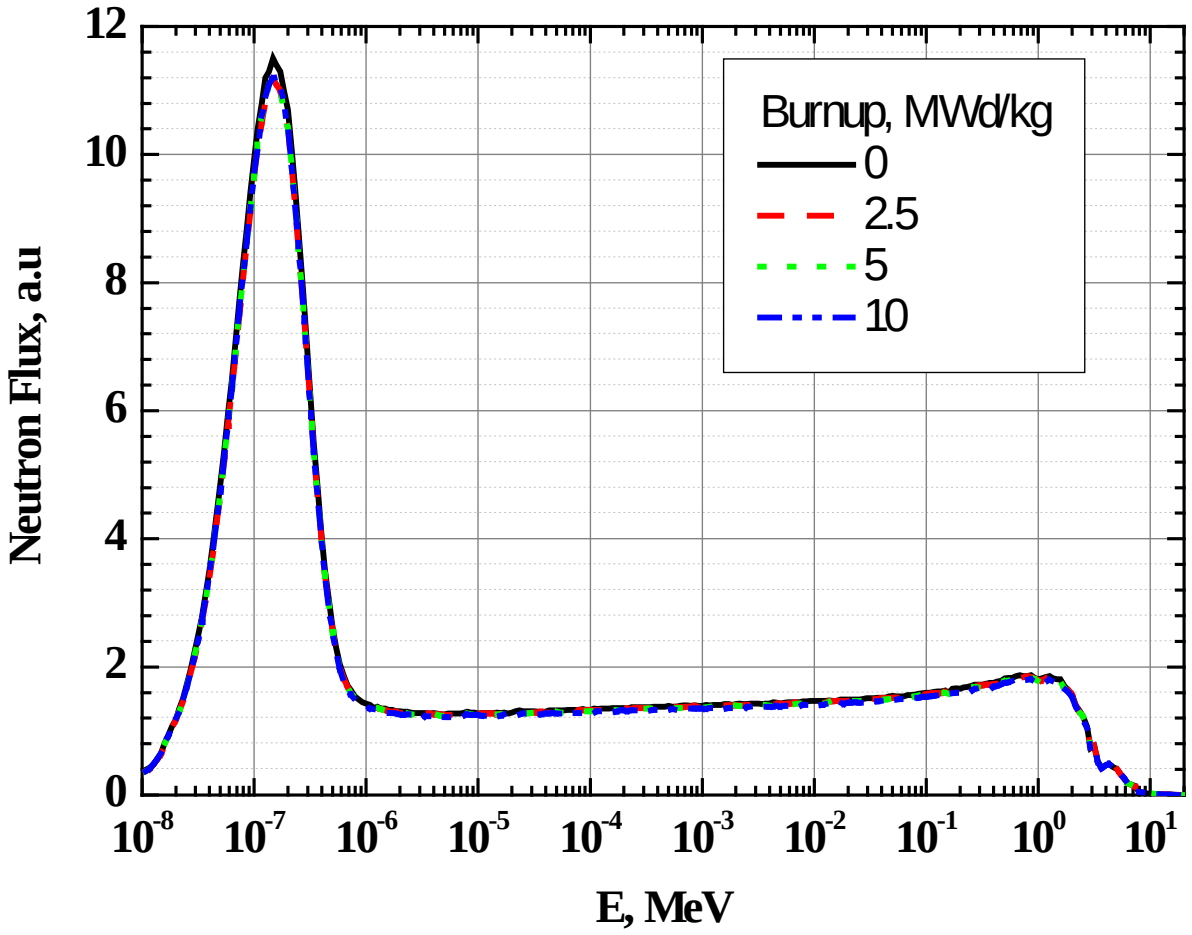

Fig. 11. Neutron energy spectrum in the graphite stack for different burn-up

2.4.2 Sampling and experimental equipment

The graphite samples from a fuel channel of the RBMK-1500 reactor have been taken to represent top, central, and bottom parts of a graphite sleeve. The graphite of the particular fuel channel of 10700 MWd burn-up, which corresponds to 11.6 years of irradiation at the average power, has been selected for sampling and modelled.

3 irradiated samples Gr.13 and Gr.14 have been taken from the central part (at the active height of ~375 cm) of the graphite sleeve of the fuel channel and 2 other samples Gr.18 and Gr.16 – from the top (at the active height of 28 cm) and the bottom (the plug fragment) of the fuel channel graphite (see Fig. 12). The sample Gr.16 (146 g) taken from the bottom part of the fuel assembly is presented in Fig. 13. The other samples weighted 2 g each. The small part of the samples has been separated and ground into the thin particles of about 200 μm of diameter. Totally 4 irradiated graphite samples and 2 reference samples of virgin graphite have been

measured using IRMS technique. Every sample has been divided into three parts and the standard measurement deviation based on a sample has been estimated.

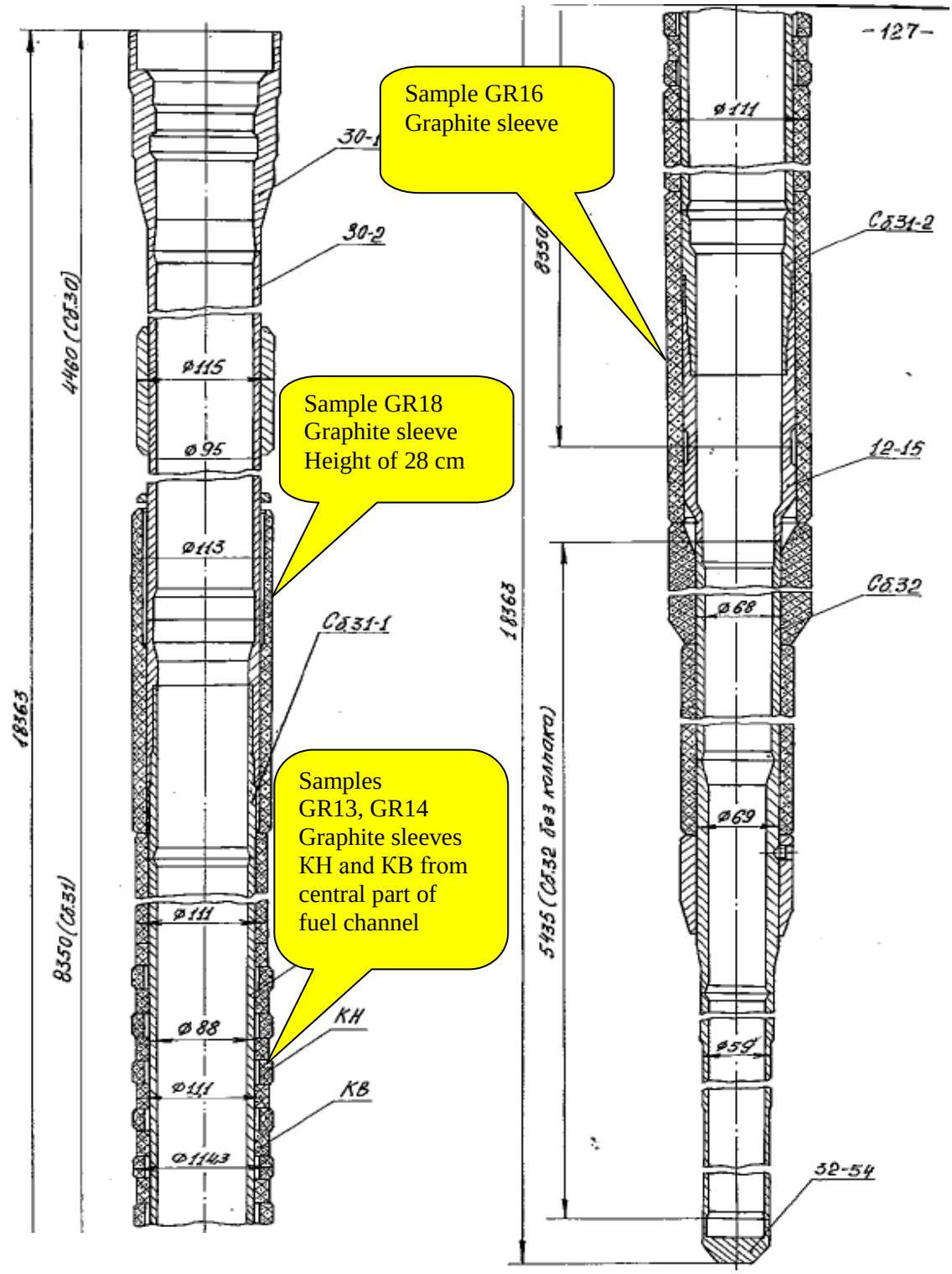

Fig. 12. Top (on the left side) and bottom parts of the fuel channel

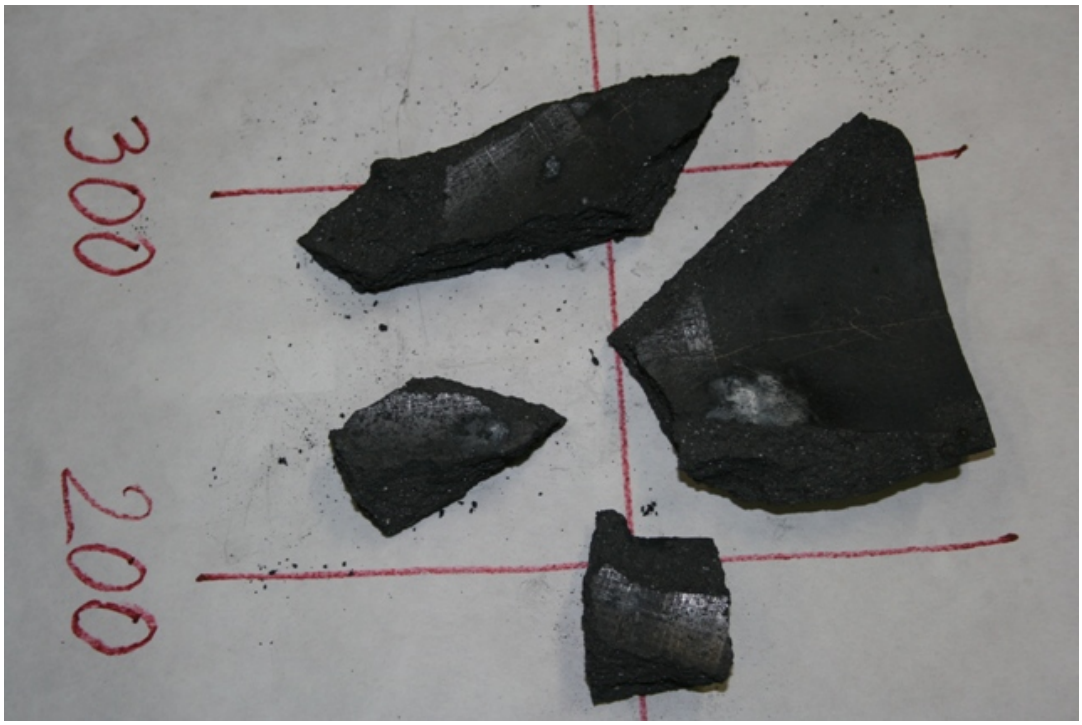

Fig. 13. The biggest (146g) sample (Gr.16) of irradiated graphite taken from the bottom part of the fuel assembly

Measurements of carbon isotopic composition of graphite have been made with the Thermo Scientific Elemental Analyzer (FlashEA 1112) connected to a stable isotope ratio mass spectrometer (Thermo Finnigan Delta Plus Advantage). Carbon analysis has been performed after sample combustion in an oxidation furnace at the temperature of 1293 K and with the oxygen excess. For more details see [18].

All carbon isotope data are reported in the delta notation $\delta^{13}C$ or differences from the given standards, expressed in parts per thousand (‰) and are calculated according to the formula:

$$\delta^{13}C = [R_{sample}/R_{standart} - 1] \times 103, ‰ \quad (2)$$

where R_{sample} = $[^{13}C]/[^{12}C]$ of the sample, $R_{standard}$ = $[^{13}C]/[^{12}C]$ of the standard (Pee Dee Belemnite (PDB), a carbonate formation, whose generally accepted absolute ratio of $[^{13}C]/[^{12}C]$ is 0.0112372± 0.0000090). Analytical precision and calibration of used reference gas CO_2 to PDB ($\delta^{13}C$ = -41.10 ± 0.08 ‰) have been estimated by the repeated analysis of certified reference material BCR 657, which gave an average value of $\delta^{13}C$ equal to -10.76 ‰ (certified value $\delta^{13}C$ = -10.76±0.04 ‰) and standard deviation equal to 0.08 ‰ Three analysis

runs of graphite samples Gr.11, Gr.12, Gr.13, Gr.14, Gr.16 and seven ones for sample Gr.18 have been performed. The sample size was approximately 300 μg. Measurement uncertainty includes scatter of measurement results and uncertainty due the reference gas tank calibration.

Graphite samples have been prepared for the quantitative analysis of ^{14}C with the liquid scintillation counter Quantulus-1220 (Wallac) by using the wet acidifying procedure with two catches ensuring 94% chemical recovery of radiocarbon [17]. For the destruction and dissolving of graphite, concentrated acids H_2SO_4, HNO_3 and $HClO_4$ (ratio 4:1:1, respectively) have been used. It should be noted that not all the material was completely dissolved by this method. After filtering, the residue has been dried, its mass has been determined, and the fraction of dissolved graphite has been estimated.

2.4.3 Evaluation of the integral neutron flux

The value of neutron flux modelled with MCNPX was $1.40 \cdot 10^{14}$ n/cm^2·s and $1.44 \cdot 10^{14}$ n/cm^2·s in the graphite sleeve and the graphite stack, respectively. The value of averaged neutron flux in the bottom and the top parts of the graphite reflector (50 cm above and below the core, respectively) is equal to $1.57 \cdot 10^{13}$ n/cm^2·s.

Concentrations of carbon isotopes in different graphite constructions calculated by modelling reactions $^{12}C(n,\gamma)^{13}C$ and $^{13}C(n,\gamma)^{14}C$ as a function of irradiation time is presented in Table 1.

Table 1. Concentrations of carbon isotopes in the graphite stack, sleeve, top and bottom reflectors modelled by reactions $^{12}C(n,\gamma)^{13}C$ and $^{13}C(n,\gamma)^{14}C$ as a function of irradiation time.

t, years	[^{14}C] ×10^{15}, at/cm^3			[^{13}C] ×10^{15}, at/cm^3		
	Stack	Sleeve	Reflectors	Stack	Sleeve	Reflectors
1	1.6	1.3	0.2	5.9	4.8	0.8
2	3.2	2.6	0.4	11.8	9.6	1.7
5	7.9	6.5	1.1	29.4	24	4.1
10	15.8	13.1	2.2	58.9	48	8.3
11.6	18.4	15.2	2.5	68.3	55.7	9.6
15	23.7	19.6	3.3	88.3	72	12.4
20	31.6	26.1	4.4	117.7	96	16.5

The results show that concentrations of ^{13}C and ^{14}C substantially increase during the reactor operation time, i.e. these isotopes accumulate in the irradiated graphite. Accumulation of ^{13}C and ^{14}C is similar in the graphite stack and sleeve, whereas it is considerably lower in the

peripheral core parts (top and bottom reflectors), which corresponds to the distribution of neutron flux.

Time dependences of both concentrations are nearly linear as the considered period of time and production rates are relatively small. In general, dynamics of accumulation of ^{13}C and ^{14}C is different. ^{13}C is produced by the $^{12}C(n,\gamma)^{13}C$ reaction and disappears by the $^{13}C(n,\gamma)^{14}C$ reaction. As the first one is faster, enhanced accumulation of ^{13}C in comparison to ^{14}C for the given period of time is observed. Meanwhile ^{14}C is a long-lived radionuclide, therefore a long time is needed to reach the equilibrium between its production and decay.

The change of a value of the ratio ($\Delta[^{13}C]/[^{12}C]$) between the irradiated and reference (virgin) graphite has been obtained by measuring $\delta^{13}C$ values in the corresponding graphite samples by the isotope mass spectrometry technique [20]. The experimentally obtained $\delta^{13}C$ values in irradiated graphite samples (Gr.13, Gr.14, Gr.16, and Gr.18) and reference samples (Gr.11 and Gr.12) are presented in Fig. 14.

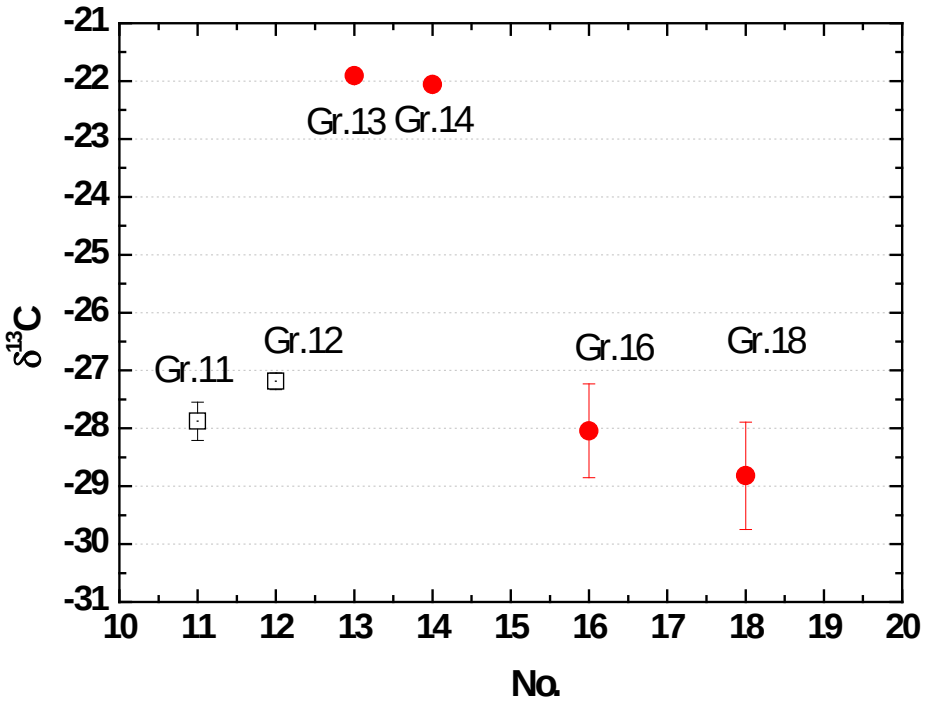

Fig. 14. $\delta^{13}C$ values measured in irradiated graphite samples (Gr.13, Gr.14, Gr.16, and Gr.18) and reference samples (Gr.11 and Gr.12)

One can see that on the basis of the ratio $\delta^{13}C$ one can clearly distinguish between the non-irradiated (Gr. 11, Gr. 12) or low-irradiated (Gr. 16, Gr. 18) and irradiated (Gr. 13, Gr. 14)

graphite samples. The difference is caused by the increased amount of ^{13}C due to its production by activation of ^{12}C.

In principle, results of mass spectrometry measurements together with an output of the computer modelling allow to draw conclusions about neutron flux in graphite constructions and graphite irradiation time or location of graphite sample in the core. These parameters are interdependent; therefore it is important to have some information about the sample in order to avoid ambiguity of evaluated parameters.

The precision of the isotope ratio mass spectrometer is <0.15 ‰ (it corresponds to the uncertainty of samples Gr.13 and Gr.14), i.e., it allows determination of $\delta^{13}C$ with sufficient accuracy from the point of view of characterization of the reactor graphite. The errors of samples Gr.16 and Gr.18 indicated in Fig. 14 are mostly determined by the sampling process: separation of small graphite particles from bulk graphite and their grinding before combustion have certain influence on the final results.

The measured change of a value of the ratio $\Delta([^{13}C]/[^{12}C])$ between virgin graphite (samples Gr.11, Gr.12) and irradiated graphite in the central area of the graphite sleeve from the fuel assembly of the RBMK-1500 reactor (samples Gr.13, Gr.14) agrees with the simulated value obtained for the graphite sleeve after 11.6 years of irradiation at the average power (see Table 2 for details). This fact confirms suitability of proposed method, i.e. it is possible using the results ($\delta^{13}C$ values) of rather simple IRMS technique and the results the computer modelling of the reactor core to draw realistic conclusions about the integral neutron flux of graphite samples of interest. The determined integral neutron flux can be used further for evaluation of radionuclide composition of graphite provided the impurities are known.

Table 2. Calculated and experimental (IRMS) changes of ratios $\Delta([^{13}C]/[^{12}C[)$ in graphite constructions after 11.6 years of irradiation in the RBMK-1500 reactor core

$\Delta([^{13}C]/[^{12}C]) \times 10^{-5}$	**Graphite constructions**			
	Stack	**Sleeve (Gr. 13 14)**	**Top reflector (Gr.18)**	**Bottom reflector (Gr. 16)**
Simulated value	7.4	6.1	1.0	1.0
Experimental value		6.2±0.1	-1.5±1.0	-0.6±0.9

The agreement between the experimental values and the modelling results for the samples from the top and the bottom reflectors (Gr.18 and Gr.16) is satisfactory. It is important to take into account that for better statistics of Monte Carlo method, modelling of neutron flux in the top and the bottom graphite reflectors has been done for a relatively large region of 50 cm height and can not precisely represent the exact neutron flux in a narrow sampling area. Moreover, samples have been taken from the top reflector at the active height of 28 cm and from the bottom reflector at an unknown position (the plug fragment), which may also have influence on the neutron flux profile and the modelling accuracy.

3 Initial material composition

Although reactor graphite is a relatively pure material, the concentration of the most part of impurities is at ppm level and below, there are still enough impurities to produce by activation numerous difficult-to-measure radionuclides. Such minor impurities in virgin graphite could not be measured with common atomic emission spectrometers or by various X-ray fluorescence techniques. As there are tens of important elements which have to be measured for modeling short- and long-lived waste, not all of them could be measured by sensitive but expensive neutron activation analysis as well. Concentrations of minor impurities in different places of the same reactor graphite construction could be in the wide range [21]. Therefore it is necessary to make many measurements in order to characterize adequately the graphite waste from a reactor. Thus, application of a rapid and a relatively cheap high resolution ICP-MS technique for measuring of minor concentrations of elements in the graphite matrix could be promising. It is important to determine precision of the mass spectrometric technique to measure concentrations of important minor impurities in the reactor graphite. For this aim results of measurements by ICP-MS method were compared with results of measurements by X-ray fluorescence technique and results of measurements by neutron activation analysis.

3.1 Determination of impurities of the reactor graphite by mass spectrometric technique

3.1.1 Preparation of samples

The sample was taken from spare ring part of graphite sleeve of the RBMK-1500 reactor fuel channel.

For X-ray fluorescence measurement, 10 g of the sample was ground for 3 minutes with the mill made of stainless steel till homogeneous powder appeared. After that the sample powder was squeezed to the (3x1) cm cylinder shape tablet (glue was not used) and placed into the X-ray spectrophotometer.

For ICP-MS measurements, as graphite is a material tough to dissolve completely even in a microwave oven, a piece of graphite ring was poured with 10 mL of 2 % nitric acid (p. a. grade, “Stanchem”, Poland), closed with a parafilm tape and left for 72 hours. After that 5 mL of solution were taken and diluted up to 15 mL with distilled water (NANOpure Barnstead/Thermolyne Co., USA). It is worth to mention that, there were plenty efforts to dissolve graphite completely by using HF acid, mixtures of H_2SO_4 and $HClO_4$ with V_2O_5, H_2SO_4 and HNO_3 with V_2O_5 (all chemicals were p. a. grade) using slight and moderate heating but extremely significant sample contaminations reaching up to (50-70) % of the signal level were observed. Nevertheless, as graphite is a porous material, it was assumed that impurities should partly or even completely wash out from the graphite sample.

3.1.2 Instruments

X-ray fluorescence analysis was carried out with the wavelength dispersive X-ray fluorescence spectrophotometer S4 Pioneer (Bruker) using factory default measurement options.

ICP-MS measurements were performed with a double focusing high resolution sector field inductively coupled plasma mass spectrometer Element 2 (Thermo Scientific). For the solution-based analysis Multi-Element standard solution VI CertiPUR (Merck, Darmstadt, Germany) at the concentration of 1 ng g−1 was used for the optimization and calibration of the ICP-MS instrument. Optimized Element 2 ICP-MS operating conditions and data acquisition parameters are summarized in Table 3.

Table 3. Optimized Element 2 ICP-MS operating conditions and data acquisition parameters

Operating conditions	
Forward power (W)	1100
Cooling gas flow rate (L min^{-1})	14.0
Auxiliary gas flow rate (L min^{-1})	0.75
Nebulizer gas flow rate (L min^{-1})	1.32
Solution uptake rate (mL min^{-1})	0.70 (peristaltic pump)
Nebulizer type	Conical U-type 1mL min^{-1} (Glass expansion)
Spray chamber type	Cyclonic of 50 ml volume (Glass expansion)
Data acquisition	
Resolution (m/Δm)	4000 (medium)
Runs and passes	10x1
Mass window (%)	300
Samples per peak	15
Search window (%)	150
Integration window (%)	80
Sampling time (s)	0.01
Integration type	Average
Scan type	E-scan

As extract from the graphite sample in the form of solution was the main test sample, standard solutions were of importance for analytical calibration of the instrument. However, for solutions only part of elements could be covered by acceptable standards. In addition, determination of percentage of the mass of elements dissolved from the graphite was another problem. Because of this, Fe was used as an internal standard, and the obtained concentration value from ICP-MS for this element was normalized to the value obtained by X-ray fluorescence technique.

Instrument response curve, obtained from the measurements of Merck VI standard solution at known concentrations of low ionization potential elements (Fig. 15) as in [22], was used for normalization of the signals of different elements.

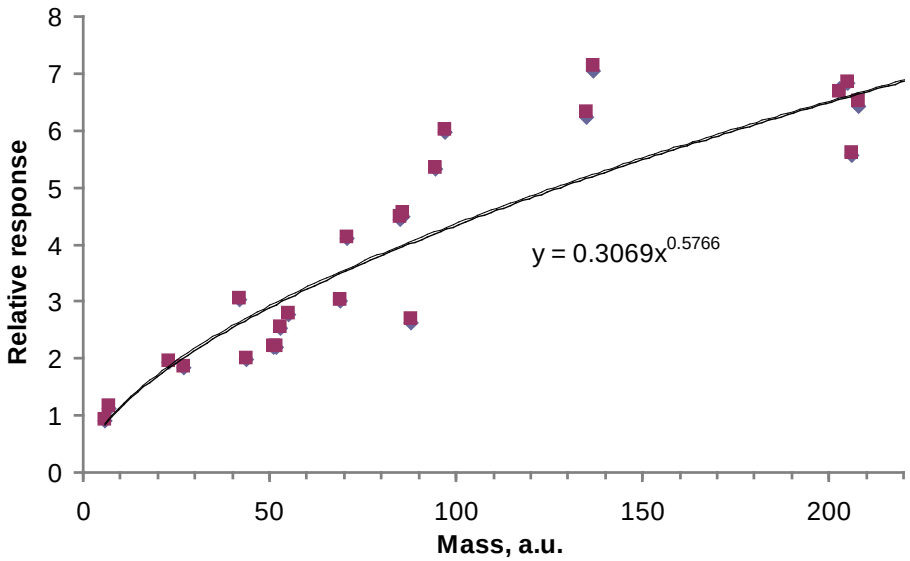

Fig. 15. Mass spectrometer Element 2 response dependence on atomic mass

Corrections because of the difference of ionization potentials were introduced according to Saha equation if appropriate (at temperature of 7700 K and electron density of $3 \cdot 10^{15}$ cm^{-3} as obtained from measurement).

3.1.3 Results

The concentration of graphite impurities measured by ICP-MS technique was compared with previously done neutron activation measurements (measured by gamma spectrometry) [7]. Results on the concentrations of elements are provided in Table 4.

Table 4. Comparison of ICP-MS results with neutron activation analysis

Element	ICP-MS		Neutron activation analysis [7, 23]	
	Concentration, g/g	Rel. unc. (%)	Concentration, g/g	Rel. unc. (%)
C	Matrix			
Li	3.9E-08	13.4	-	-
B	9.6E-06	1.8	-	-
Na	3.6E-05	4.2	4.6E-06	6.3
Mg	2.8E-06	12.5	7.0E-06	-
Al	1.1E-05	2.9	9.2E-06	1.3
Si	7.8E-05	7.1	-	-
P	1.9E-06	3.1	-	-
S	4.7E-05	2.2	-	-

Cl	1.6E-05	7.9	7.6E-06	2.3
K	2.2E-05	2.0	1.9E-06	12.0
Ca	7.5E-05	4.1	5.2E-05	4.3
Ti	3.8E-06	3.9	1.7E-05	2.7
V	1.9E-07	4.0	1.7E-05	1.3
Cr	4.7E-07	5.5	6.0E-07	1.7
Mn	5.9E-07	3.4	5.8E-07	1.7
Fe	4.1E-05	4.1	1.9E-05	5.3
Co	3.5E-08	11.3	1.9E-08	0.7
Ni	6.1E-07	4.4	3.9E-07	8.3
Cu	6.6E-07	3.4	-	-
Zn	2.7E-06	3.6	2.0E-08	-
Ga	4.3E-09	37.8	1.0E-08	-
Ge	2.1E-09	200.2	9.0E-06	-
Sr	1.1E-06	5.8	9.6E-07	5.7
Zr	7.3E-07	7.4	1.0E-06	7.0
Nb	6.0E-09	14.2	-	-
Mo	5.8E-08	26.6	1.7E-07	0.7
Ag	6.5E-08	14.1	3.0E-09	20.0
Cd	3.4E-08	26.1	1.5E-08	-
Sn	1.4E-07	12.6	1.5E-07	-
Cs	2.1E-09	33.6	1.6E-09	9.3
Ba	1.3E-06	1.4	2.0E-06	2.3
Eu	2.3E-09	50.0	2.6E-09	2.0
Ho	2.1E-09	38.1	9.4E-09	6.7
Hf	1.5E-08	24.4	5.8E-09	1.7
Ta	2.4E-10	104.2	1.9E-09	3.3
W	4.2E-08	11.8	4.7E-08	3.7
Pb	2.1E-06	8.2	-	-
Bi	1.7E-09	30.2	-	-
Th	3.4E-09	26.4	7.9E-09	1.7
U	5.4E-09	18.8	1.6E-08	2.7

Concentrations of 40 elements were measured by ICP-MS technique. As seen from Table 2, almost all concentrations of elements determined by mass spectrometry are of the same order as the values measured by the neutron activation analysis technique. Such measurement precision is enough for radioactive waste characterization. Concentrations of a few elements such as Na, K, Ti, V, Zn, Ga, Ge, Ag, and Ta measured by various methods showed too much different results.

Concentrations of Na and K observed in ICP-MS analysis results were higher by one order than ones measured by neutron activation analysis technique. These elements are very common in the environment, thus higher concentrations could be influenced by contamination of the sleeve by Na and K during usual its handling in the Ignalina NPP as this spare part was stored in ordinary conditions there.

It was found, that Ti, V, Ga, Ge, and Ta concentration values were lower in one order (Ge – in three orders) than measured ones by neutron activation analysis. This could happen because the elements did not wash out from the graphite matrix as well as other elements because of lower solubility. Besides, higher concentration of Zn was also observed in ICP-MS analysis. Higher concentration by two orders of magnitude could be influenced by contamination of a parafilm tape used as it contains significant amount of Zn [24]. However, higher Ag concentration by one order than in neutron activation results shows that the neutron activation value having comparatively high RSD could be undervalued.

It seems that Cl, important element for modeling long-lived graphite waste, can be successfully measured by ICP-MS technique. Cl is a tough element to be measured by ICP-MS due to high contamination from the environment and chemicals used for the preparation of a sample. Nevertheless, in spite that the background/signal ratio was high (up to 47%) in comparison with other elements, the contamination influence was stable and thus Cl concentration can be included into the measurement results.

3.1.4 Conclusions

The most important elements for evaluation of short- and long-lived activation products in the irradiated RBMK-1500 graphite by simulation of activation were measured with the accuracy sufficient for the characterization of radioactive waste. Fe concentration obtained by X-ray fluorescence technique was used as an internal standard for normalization of the ICP-MS measurement results. Concentrations of the most elements measured by ICP-MS analysis shows acceptable agreement with the concentrations determined by neutron activation method. In this work it has been shown that ICP-MS is a promising technique for determination of concentration of graphite minor impurities as it is a rapid and a relatively cheap method.

3.2 Comparison of available data on impurities in RBMK-1500 reactor virgin graphite

Activity inventories were estimated for the graphite blocks and graphite rings/sleeves as indicated in Table 5.

Table 5. Construction materials of the RBMK-1500 reactor components being analyzed

Reactor Component	Structural Element	Material of Construction	Mass (tones)
Graphite stack	Graphite blocks Graphite rings/sleeves	Graphite GR-280 Graphite GRP-2-125	~1800 ~100

Chemical composition and concentrations of the elements (main elements and impurities) of these reactor parts were defined based on the data presented in available scientific and technical literature for the specific material being analyzed. It was assumed that the isotopic composition of each chemical element is the same as the naturally occurring isotopic content. Due to the lack of representative information on the material composition of the reactor structural components of Ignalina NPP and in order to assess the impact of the impurities on the induced activity (i.e. to assess the range of induced activity variation of these structural components depending on the initial impurities content), two cases (Case A and Case B) were defined for the neutron activation analysis:

- Materials' composition with maximal concentration of impurities is assumed for each of structural components being analyzed (Case A);
- Materials' composition with minimal concentration of impurities is assumed for each of structural components being analyzed (Case B).

Maximal and minimal impurities concentrations in GR-280 and GRP-2-125 grade graphite gathered from available published sources are presented in Table 6 and Table 7, respectively. These chemical compositions were used for graphite neutron activation assessment in this study.

Table 6. Chemical composition of reactor RBMK-1500 graphite blocks (with impurities) [3–6]

Graphite GR-280					
Element	**Max. weight fraction (%)**	**Min. weight fraction (%)**	**Element**	**Max. weight fraction (%)**	**Min. weight fraction (%)**
Ag	$3.90\cdot10^{-6}$	$3.00\cdot10^{-7}$	Li	$1.00\cdot10^{-3}$	$4.00\cdot10^{-7}$
Al	$9.00\cdot10^{-5}$	$2.00\cdot10^{-6}$	Mg	$1.70\cdot10^{-2}$	$1.00\cdot10^{-6}$
As	$2.00\cdot10^{-5}$	$3.00\cdot10^{-6}$	Mn	$9.00\cdot10^{-5}$	$5.00\cdot10^{-7}$
Au	$3.00\cdot10^{-7}$	$2.00\cdot10^{-8}$	N	$7.00\cdot10^{-3}$	$4.00\cdot10^{-5}$
B	$4.00\cdot10^{-5}$	$4.00\cdot10^{-6}$	Na	$2.30\cdot10^{-3}$	$8.00\cdot10^{-4}$
Bi	$3.00\cdot10^{-6}$	$3.00\cdot10^{-6}$	Ni	$3.00\cdot10^{-5}$	$4.00\cdot10^{-7}$
Br	$5.00\cdot10^{-6}$	$2.00\cdot10^{-7}$	O	$1.80\cdot10^{-4}$	$1.80\cdot10^{-4}$
C	Remain. part	Remain. part	Pb	$1.00\cdot10^{-5}$	$1.00\cdot10^{-5}$
Ca	$1.00\cdot10^{-2}$	$4.00\cdot10^{-6}$	Sb	$1.10\cdot10^{-6}$	$2.00\cdot10^{-7}$
Cd	$3.00\cdot10^{-5}$	$3.00\cdot10^{-5}$	Sc	$3.00\cdot10^{-7}$	$4.00\cdot10^{-9}$
Cl	$3.20\cdot10^{-3}$	$1.00\cdot10^{-5}$	Se	$1.40\cdot10^{-7}$	$3.00\cdot10^{-8}$
Co	$6.30\cdot10^{-6}$	$1.20\cdot10^{-7}$	Si	$4.70\cdot10^{-3}$	$7.00\cdot10^{-5}$
Cr	$4.00\cdot10^{-5}$	$1.00\cdot10^{-7}$	Sn	$1.00\cdot10^{-5}$	$1.00\cdot10^{-5}$
Cs	$2.00\cdot10^{-5}$	$2.00\cdot10^{-8}$	Th	$2.00\cdot10^{-5}$	$3.00\cdot10^{-8}$
Cu	$3.00\cdot10^{-6}$	$1.00\cdot10^{-6}$	Ti	$8.00\cdot10^{-6}$	$3.00\cdot10^{-6}$
Eu	$3.00\cdot10^{-5}$	$3.00\cdot10^{-5}$	U	$2.00\cdot10^{-5}$	$1.00\cdot10^{-6}$
Fe	$9.40\cdot10^{-3}$	$2.00\cdot10^{-6}$	V	$5.00\cdot10^{-6}$	$1.30\cdot10^{-6}$
H	$1.10\cdot10^{-4}$	$1.10\cdot10^{-4}$	W	$4.00\cdot10^{-4}$	$4.00\cdot10^{-6}$
Hg	$2.90\cdot10^{-6}$	$2.50\cdot10^{-6}$	Zn	$1.72\cdot10^{-4}$	$3.00\cdot10^{-5}$
K	$2.50\cdot10^{-3}$	$3.00\cdot10^{-4}$			

Table 7. Chemical composition of reactor RBMK-1500 graphite rings/sleeves [5–7]

Graphite GRP-2-125					
Element	**Max. weight fraction (%)**	**Min. weight fraction (%)**	**Element**	**Max. weight fraction (%)**	**Min. weight fraction (%)**
Ag	$6.00\cdot10^{-6}$	$3.00\cdot10^{-7}$	Mg	$1.70\cdot10^{-2}$	$5.00\cdot10^{-5}$
Al	$9.20\cdot10^{-4}$	$1.00\cdot10^{-4}$	Mn	$5.00\cdot10^{-4}$	$2.00\cdot10^{-5}$
Ar	$1.40\cdot10^{-5}$	$1.40\cdot10^{-5}$	Mo	$1.70\cdot10^{-5}$	$1.70\cdot10^{-5}$
As	$4.50\cdot10^{-6}$	$1.10\cdot10^{-6}$	Na	$5.00\cdot10^{-4}$	$4.64\cdot10^{-4}$
Au	$7.30\cdot10^{-8}$	$2.20\cdot10^{-8}$	Nd	$1.10\cdot10^{-5}$	$1.10\cdot10^{-5}$
B	$3.00\cdot10^{-4}$	$5.00\cdot10^{-6}$	Ni	$3.90\cdot10^{-5}$	$3.00\cdot10^{-5}$
Ba	$2.01\cdot10^{-4}$	$2.01\cdot10^{-4}$	P	$5.00\cdot10^{-5}$	$5.00\cdot10^{-5}$
Br	$2.50\cdot10^{-6}$	$2.50\cdot10^{-6}$	Pr	$8.00\cdot10^{-6}$	$8.00\cdot10^{-6}$
C	Remain. part	Remain. part	Rb	$8.00\cdot10^{-7}$	$8.00\cdot10^{-7}$
Ca	$5.19\cdot10^{-3}$	$1.00\cdot10^{-4}$	Re	$1.90\cdot10^{-7}$	$1.90\cdot10^{-7}$
Cd	$1.50\cdot10^{-6}$	$1.50\cdot10^{-6}$	Ru	$7.00\cdot10^{-6}$	$7.00\cdot10^{-6}$
Ce	$2.69\cdot10^{-5}$	$2.69\cdot10^{-5}$	Sb	$2.70\cdot10^{-6}$	$1.00\cdot10^{-7}$
Cl	$1.04\cdot10^{-3}$	$3.10\cdot10^{-4}$	Sc	$5.00\cdot10^{-6}$	$5.00\cdot10^{-9}$
Co	$5.30\cdot10^{-6}$	$9.00\cdot10^{-8}$	Se	$3.00\cdot10^{-7}$	$5.00\cdot10^{-8}$
Cr	$1.00\cdot10^{-4}$	$5.00\cdot10^{-8}$	Si	$1.00\cdot10^{-4}$	$1.00\cdot10^{-4}$
Cs	$4.90\cdot10^{-7}$	$2.00\cdot10^{-8}$	Sm	$2.13\cdot10^{-6}$	$2.13\cdot10^{-6}$
Cu	$1.00\cdot10^{-5}$	$1.00\cdot10^{-5}$	Sn	$1.50\cdot10^{-5}$	$1.50\cdot10^{-5}$
Dy	$3.20\cdot10^{-7}$	$3.20\cdot10^{-7}$	Sr	$9.60\cdot10^{-5}$	$9.60\cdot10^{-5}$
Er	$5.30\cdot10^{-7}$	$5.30\cdot10^{-7}$	Ta	$1.90\cdot10^{-7}$	$1.90\cdot10^{-7}$
Eu	$2.60\cdot10^{-7}$	$2.60\cdot10^{-7}$	Tb	$2.70\cdot10^{-7}$	$2.70\cdot10^{-7}$
Fe	$5.80\cdot10^{-3}$	$1.00\cdot10^{-4}$	Te	$1.40\cdot10^{-6}$	$1.40\cdot10^{-6}$
Ga	$1.00\cdot10^{-6}$	$1.00\cdot10^{-6}$	Th	$8.40\cdot10^{-7}$	$3.00\cdot10^{-8}$
Ge	$9.00\cdot10^{-4}$	$9.00\cdot10^{-4}$	Ti	$1.74\cdot10^{-3}$	$1.74\cdot10^{-3}$
Hf	$5.80\cdot10^{-7}$	$5.80\cdot10^{-7}$	Tm	$5.60\cdot10^{-7}$	$5.60\cdot10^{-7}$
Hg	$4.10\cdot10^{-6}$	$6.20\cdot10^{-8}$	U	$1.10\cdot10^{-5}$	$1.60\cdot10^{-6}$
Ho	$9.40\cdot10^{-7}$	$9.40\cdot10^{-7}$	V	$1.74\cdot10^{-3}$	$1.74\cdot10^{-3}$
I	$4.00\cdot10^{-6}$	$4.00\cdot10^{-6}$	W	$2.10\cdot10^{-4}$	$4.70\cdot10^{-6}$
In	$3.00\cdot10^{-7}$	$3.00\cdot10^{-7}$	Yb	$1.40\cdot10^{-6}$	$1.40\cdot10^{-6}$
K	$1.90\cdot10^{-4}$	$1.50\cdot10^{-4}$	Zn	$8.70\cdot10^{-5}$	$2.00\cdot10^{-6}$
La	$1.50\cdot10^{-5}$	$1.50\cdot10^{-5}$	Zr	$1.00\cdot10^{-4}$	$1.00\cdot10^{-4}$
Lu	$1.50\cdot10^{-7}$	$1.50\cdot10^{-7}$			

During CARBOWASTE project two independent analyses of virgin RBMK-1500 graphite ring/sleeve samples compositions were performed. One was performed by CPST (Lithuania) – state research institute Center for Physical Sciences and Technology employing mass spectrometric determination of impurities in graphite [8], while the other was performed by Institute of Isotopes (Hungary) on request from Forschungszentrum Juelich GmbH – FZJ

(Germany) employing prompt gamma activation analysis [9]. The list of detected impurities and their quantities for both analyses generally agreed good with the results of earlier investigations, i.e. impurities concentrations in graphite samples were in the range of "Min." and "Max." or below "Min" concentrations, presented in Table 7. However, some new impurities were detected and some impurities were observed having higher concentrations, as presented in Table 8.

Table 8. List and concentrations of new impurities (and ones, having higher concentrations) in GRP-2-125 graphite samples

Element	Max. weight fraction (%) from Table 7	CPST [8]	FZJ [9]
Ag	$6.00 \cdot 10^{-6}$	$6.50 \cdot 10^{-6}$	
Al	$9.20 \cdot 10^{-4}$	$1.10 \cdot 10^{-3}$	
B	$3.00 \cdot 10^{-4}$	$9.60 \cdot 10^{-4}$	
Bi	–	$1.70 \cdot 10^{-7}$	
Ca	$5.19 \cdot 10^{-3}$	$7.50 \cdot 10^{-3}$	
Cd	$1.50 \cdot 10^{-6}$	$3.40 \cdot 10^{-6}$	$3.00 \cdot 10^{-6}$
Cl	$1.04 \cdot 10^{-3}$	$1.60 \cdot 10^{-3}$	
Cu	$1.00 \cdot 10^{-5}$	$6.60 \cdot 10^{-5}$	
Gd	–		$2.00 \cdot 10^{-6}$
H	–		$4.80 \cdot 10^{-3}$
Hf	$5.80 \cdot 10^{-7}$	$1.50 \cdot 10^{-6}$	
K	$1.90 \cdot 10^{-4}$	$2.20 \cdot 10^{-3}$	$7.00 \cdot 10^{-4}$
Li	–	$3.90 \cdot 10^{-6}$	
Na	$5.00 \cdot 10^{-4}$	$3.60 \cdot 10^{-3}$	
Nb	–	$6.00 \cdot 10^{-7}$	
Ni	$3.90 \cdot 10^{-5}$	$6.10 \cdot 10^{-5}$	
P	$5.00 \cdot 10^{-5}$	$1.90 \cdot 10^{-4}$	
Pb	–	$2.10 \cdot 10^{-4}$	
S	–	$4.70 \cdot 10^{-3}$	$9.80 \cdot 10^{-3}$
Si	$1.00 \cdot 10^{-4}$	$7.80 \cdot 10^{-3}$	
Sm	$2.13 \cdot 10^{-6}$		$3.20 \cdot 10^{-6}$
Sr	$9.60 \cdot 10^{-5}$	$1.10 \cdot 10^{-4}$	
Ti	$1.74 \cdot 10^{-3}$		$2.60 \cdot 10^{-3}$
Zn	$8.70 \cdot 10^{-5}$	$2.70 \cdot 10^{-4}$	

According to the Table 8, new impurities were observed: Bi, Gd, H, Li, Nb, Pb and S, which were not reported previously for this graphite grade. From the impurities, which had higher concentrations, the highest difference was observed for silicon (Si) and potassium (K) – concentrations were higher by 78 and 12 times respectively. For the remaining impurities concentrations differed less and differences did not exceeded 8 times.

4 Spatial and energetic neutron flux distribution

Neutron fluxes were modelled in these RBMK-1500 reactor structures:

- In the graphite blocks;
- In the graphite rings/sleeves;
- In the central FC part.

The neutron fluxes were estimated and for FC tubes i.e. their central parts made of zirconium alloy E125. These tubes are located closer to the fuel region than the graphite components and thus modelling of neutron fluxes in them was selected for the investigation of the impact of different fuel type (and burnup) and different data libraries on the modelled neutron fluxes.

The modelled neutron fluxes are presented in subsequent chapters below. For convenience purpose the axial distance from the centre of the reactor core is given in the ordinate axis in the below figures, assuming that the centre of the core is at zero mark. Modelled fluxes represents reactor operation at 4200 MW thermal power, i.e. at ~2.6 MW thermal power for one FC.

4.1 Graphite blocks

The results of the neutron flux modelling show that the thermal and resonance neutron fluxes are dominant in the graphite column (blocks); however, the thermal neutron flux is more intensive than the resonance neutron flux (though very insignificantly in certain regions), see Fig. 16.

The fast neutron flux is about 10 times lower than that of resonance neutrons and their distribution along the axial direction is the same as the resonance neutron flux variations. As it has been expected there are two maximums in the distribution profile of the fast and resonance neutron fluxes and one minimum in the distribution profile at the point in the reactor core, which corresponds to the point of the fuel bundles connection in the fuel assembly. In this region the fast and resonance neutron fluxes are app. 1.2 times lower than the maximal neutron fluxes. In the graphite column edges (reflector blocks) the fast and the resonance neutron fluxes are app. 34 (top reflector) and 28 (bottom reflector) times lower than the maximal neutron fluxes.

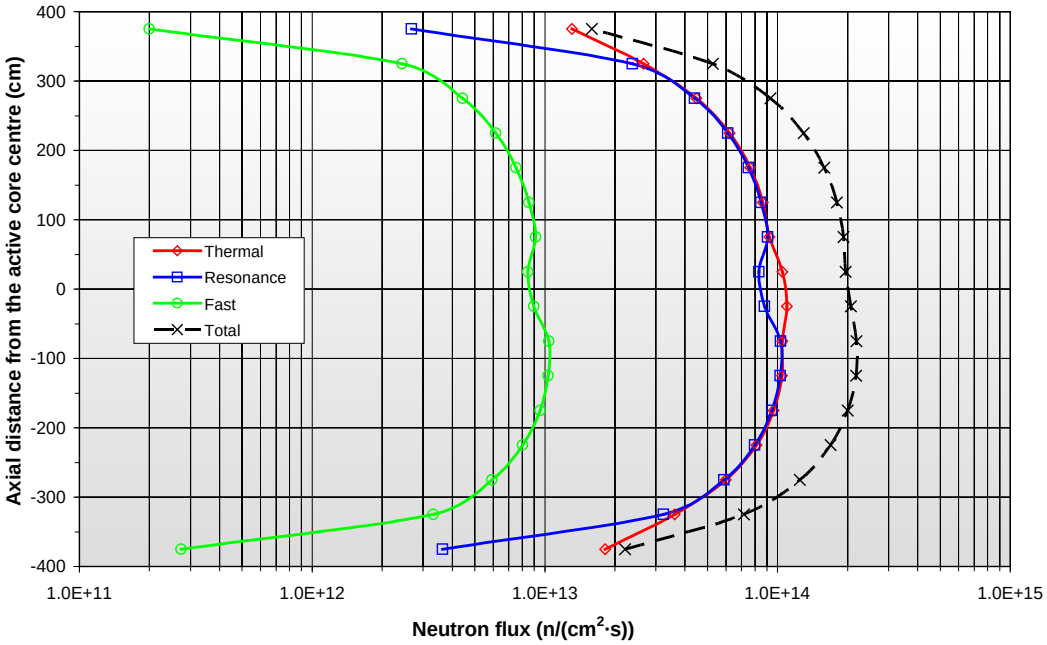

Fig. 16. Neutron fluxes in the graphite column (blocks)

In case of thermal neutron flux there is only one maximum in the neutron flux distribution profile and it is located in the central part of the reactor core. Going further from the reactor core centre the thermal fluxes decrease monotonically and in the graphite column edges i.e. top and bottom reflectors they are ~8 and ~6 times lower than the maximal flux, respectively. The average (averaged over whole the 8 m long part of graphite column) thermal neutron flux in graphite column is ~$7.0 \cdot 10^{13}$ n/cm^2·s while maximal value of thermal flux is ~$1.1 \cdot 10^{14}$ n/cm^2·s.

4.2 Graphite rings/sleeves

Similar neutron fluxes distributions are obtained and for graphite rings/sleeves in the reactor core. The results of the neutron flux modelling show that the thermal and the resonance neutron fluxes are dominant in the graphite rings/sleeves and the fast neutron flux is about 6 times lower than that of resonance neutrons (see Fig. 17). However, as distinct from graphite blocks, the resonance neutron flux is more intensive than the thermal neutron flux (except the very centre, the top and the bottom reflectors regions) in graphite rings/sleeves. The average (averaged over the 8 m long part of graphite rings/sleeves inside the graphite stack region) thermal neutron flux in graphite rings/sleeves is ~$5.7 \cdot 10^{13}$ n/cm^2·s while maximal value of thermal flux is ~$9.3 \cdot 10^{13}$ n/cm^2·s.

Comparison of neutron fluxes in the graphite bocks and rings/sleeves (see Fig. 16 and Fig. 17) gives that total and resonance neutron fluxes are almost equal in these structures, but thermal neutron flux is about 1.2 times higher in graphite blocks than in rings/sleeves whereas fast neutron flux is 1.8 times higher in the graphite rings/sleeves than in blocks.

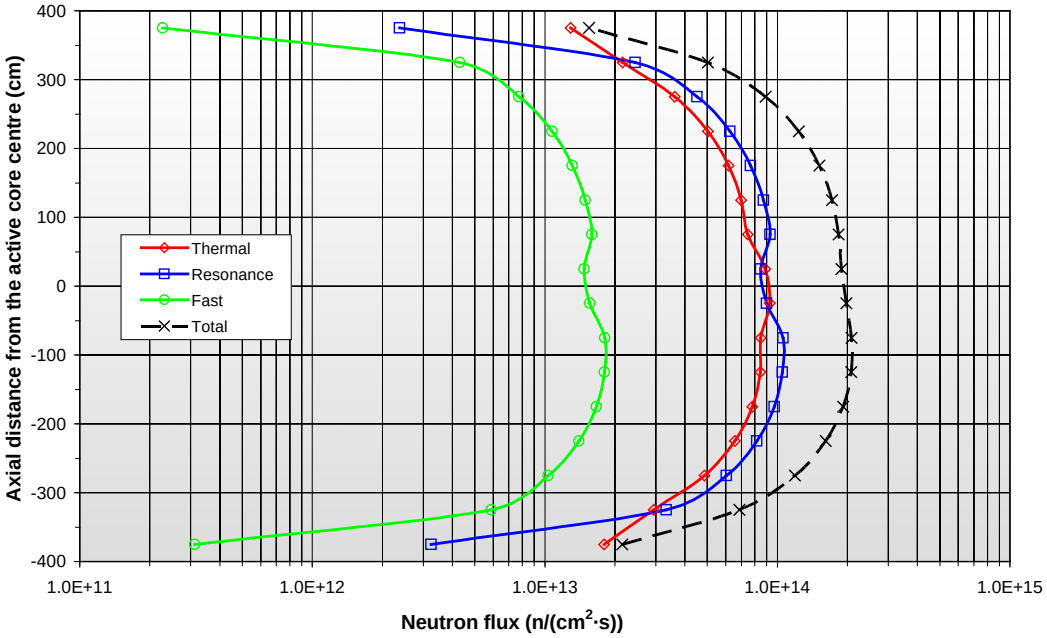

Fig. 17. Neutron fluxes in the graphite rings/sleeves

4.3 FCs central parts

The modelling results of the neutron flux variation along the central part of the fuel channel are presented in Fig. 18.

Likewise for the graphite blocks and rings/sleeves the variation of the fast and the resonance neutron fluxes along the axial direction are similar. There are two maximum (the bottom one is higher) and one minimum neutron flux points in the distribution; the later one corresponds to the point of the fuel bundles connection into the fuel assembly. The maximal thermal neutron flux is observed in the central part of the reactor core only. Going further from the reactor core centre the thermal flux decreases and in the edges it is ~7 (top) and ~5 (bottom) times lower than the maximal flux in this structural component. The average (averaged over the 8 m long central part of FC) thermal neutron flux in central part of FC is ~$5.3 \cdot 10^{13}$ n/cm^2·s while maximal value of thermal flux is ~$8.7 \cdot 10^{13}$ n/cm^2·s.

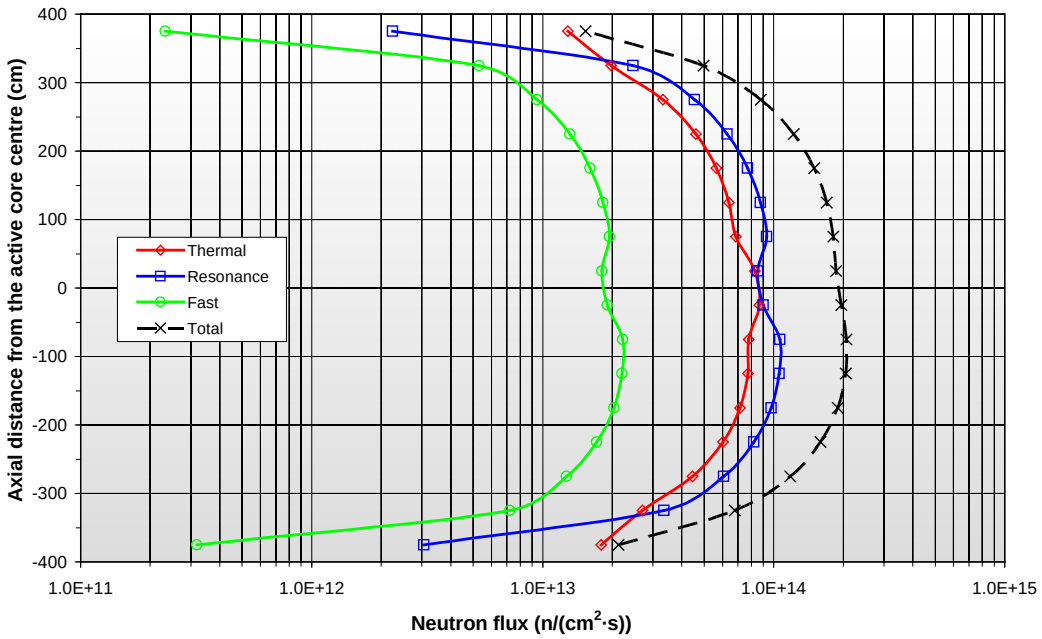

Fig. 18. Neutron fluxes in the central part of the fuel channel

The fast neutron flux in the edges of the FC central part is about 10 times and in the remaining part of the component – about 5 times lower than the resonance neutron flux. Similar to the case of the graphite rings/sleeves the resonance neutron flux is dominant in the analyzed structural component with exception in the edges (where the thermal flux is ~6 times higher) and its centre (where thermal and resonance fluxes are practically equal).

4.4 Discussion

It was already mentioned that three different cases of one lattice cell model were developed in order to analyze the impact of various factors (nuclear fuel type, burnup) on the energetic and spatial distribution of the neutron flux in the RBMK-1500 reactor structural components. To evaluate the influence of the control rods on the neutron flux distribution the second model of 16 cells was developed. The modelling results for thermal neutron flux obtained using these different modelling cases for FC central part are presented in Fig. 19.

As presented in Fig. 19, the most intensive thermal neutron flux along the axial direction is obtained using the third case of the first model where fresh fuel without erbium absorber was assumed (comparing three cases of the one lattice cell model). Minimal differences in the neutron flux density are obtained in the centre and edges and are equal to ~4 % and ~7 %,

respectively, while the largest differences are obtained in the medium parts, where they make up ~16 %. The average difference along the fuel channel is about 10 % and the neutron flux variation character is the same. The comparison of the neutron fluxes distribution obtained using the first and the second one lattice cell model cases (fuel with erbium absorber) shows that the maximal differences are obtained in the fuel channel edges (~6 %), while in the other parts the differences of the fluxes are smaller (up to 3 %). Such a variation of the neutron fluxes confirms the fact that the presence of burnable erbium absorber in nuclear fuel decreases the maximal power of fresh uranium–erbium fuel assemblies as the neutron fluxes (and thus multiplication factor) decreases due to the additional absorption of thermal neutrons. Due to erbium burnup the power of uranium–erbium fuel assemblies less varies during the operation than that of usual uranium fuel assemblies and the lower differences between the power of fuel assemblies with different burnup determine better (more even) power distribution within the reactor core.

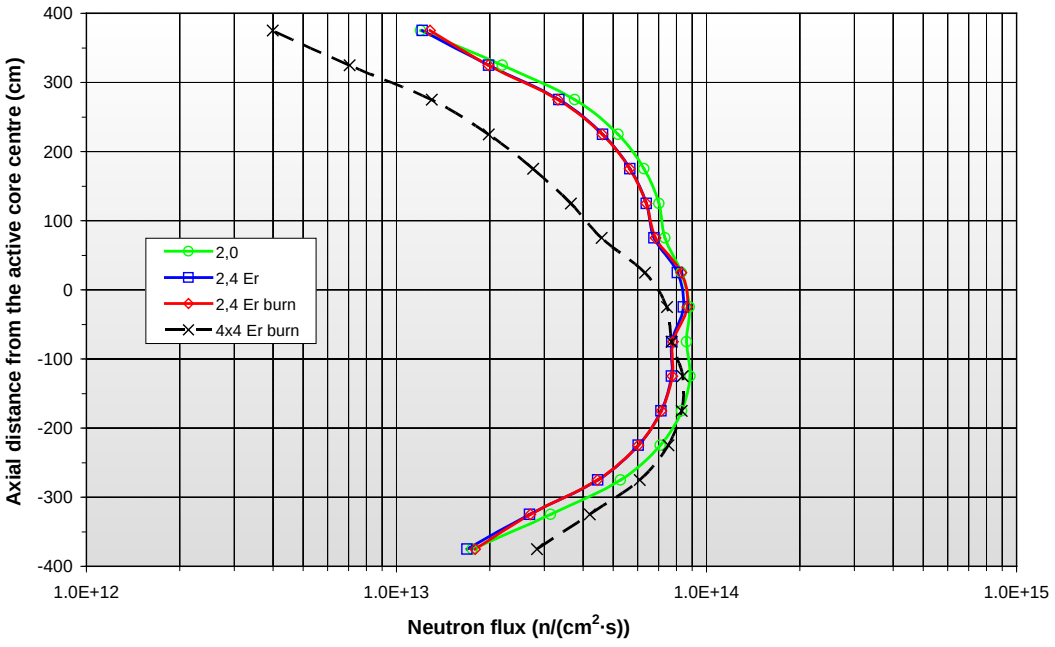

Fig. 19. Thermal neutron fluxes in FC central part

The comparison of the neutron flux modelling results obtained using the second model and the three cases of the first model shows the differences in the neutron fluxes and in their variation character as well (Fig. 19). The assessed maximal thermal neutron flux is lowest in the case of the second model (~5 % lower than that of the 3rd case of the first model) and it is obtained in

the lower part of the fuel channel. Maximal differences in comparison with the first model three cases are obtained in the top part of the FC where the thermal neutron flux is about 69 % lower, while in the bottom part of the FC the thermal neutron flux is a bit higher and the differences make up ~41 %. For the fast and resonance neutron fluxes the similar results are obtained, but not presented here. Neutron fluxes determined using the second model are lower in the top part of the FC and higher in the bottom part of the FC.

Practically, during the reactor operation the neutron flux distribution as evaluated using the second model is tried to be avoided as the power along the axial direction and in the radial direction should be distributed evenly as much as possible. Thus during the reactor operation the positions of the control rods are various and are changed depending upon fuel burnup, refuelling, etc. Besides, the control rods inserted from the reactor bottom could also be used to make the reactor power more evenly distributed in the axial direction. The situation with the fully inserted and withdrawn control rods close to each other is also hardly probable. Due to the mentioned reasons the neutron flux modelling results obtained using the second model were not used for the neutron activation modelling of the reactor structural components, but were used only for the indication of possible impact to the modelled neutron fluxes.

Radial distribution of thermal neutron fluxes obtained in the 1st case of one cell model (averaged over 50 cm height of the modelled segment in the range of -150 – -100 cm from the centre of the core) and in the second 16 cell model (averaged over 50 cm height of the modelled segment in the range of -250 – -150 cm from the centre of the core) are presented in Fig. 20 and Fig. 21 respectively.

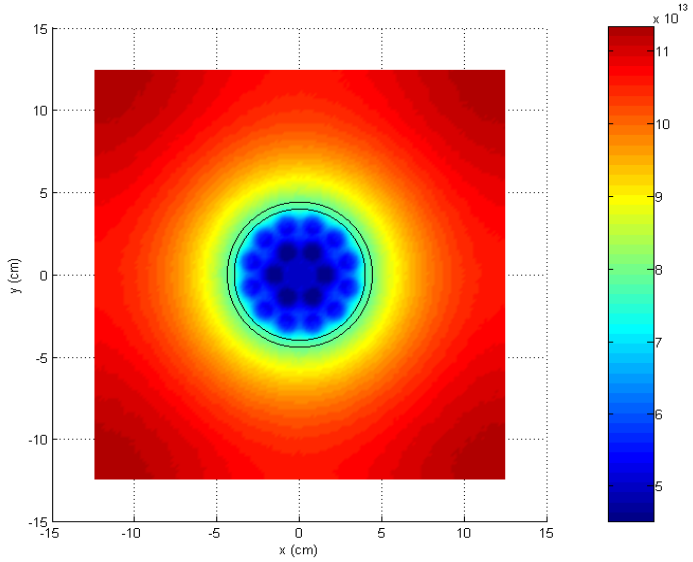

Fig. 20. Radial distribution of thermal neutron flux in the reactor RBMK-1500 one cell model

Results of one cell model (see Fig. 20) clearly shows, that thermal neutrons are dominant in the graphite block (where moderation of the fast and the resonance neutrons generally takes place), whereas in the fuel channel (marked with black circles in the Fig. 20) and graphite rings/sleeves thermal neutron fluxes are lower. The absorption of thermal neutrons in fuel elements inside the fuel channel is also well expressed, indicating 18 zones (fuel elements, see Fig. 4) where thermal neutron flux is lowest.

Similar results for cells with fuel assemblies are achieved and for second (16 cell) model, as presented in Fig. 21.

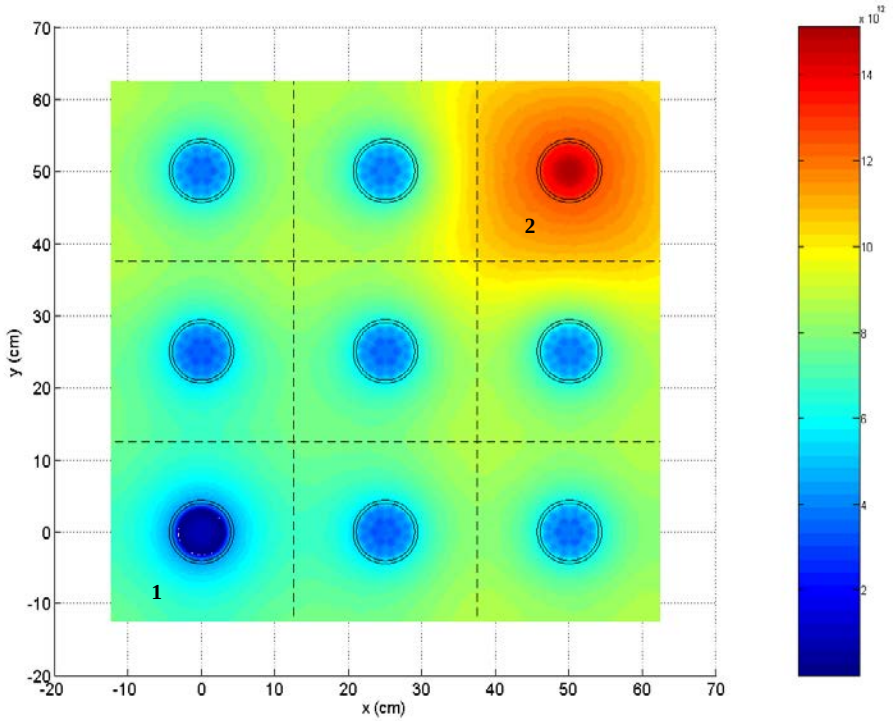

Fig. 21. Radial distribution of thermal neutron flux in the reactor RBMK-1500 16 cell model (only 9 cells shown including 2 cells with the control rods; 1 – fully inserted, 2 – fully withdrawn)

For cells with fuel assemblies, the highest thermal neutron fluxes are in the graphite blocks and decrease going from the periphery to the centre of the cell where fuel channels with fuel assemblies are located. The cell marked as “1” represents cell where control rod with neutron absorber is fully inserted in FC, whereas cell marked as “2” represents cell where control rod with neutron absorber is fully withdrawn from FC. Results for cell “1” clearly show (see Fig. 21, cell “1”) that thermal neutrons are absorbed in the control rod and thus flux inside the FC is lowest. Contrary results are achieved for cell “2”, where control rod is withdrawn from active core. The control rods are made from two potions (boron absorber and graphite portions) and are designed so, that when extracting them from the active core a portion with absorber comes out of the core and a portion with graphite takes its place. In this manner the part of coolant in FC is replaced with graphite and neutron balance is improved. Results for cell “2” clearly indicate this (see Fig. 21, cell “2”): thermal neutron flux is highest in this cell and increases going from the periphery of the cell to its centre, where additional moderation of fast and resonance neutron in the graphite part of withdrawn control rod takes place.

Additionally, the impact of different data libraries on modelled neutron fluxes was also evaluated. Three different nuclear data libraries from MCNP 5 package (ENDF/B-V, ENDF/B-VI and LLNL) were selected for that purpose. The modelling was performed for the FC central part using the first case one lattice cell model. The modelling results for thermal neutron fluxes obtained using mentioned data libraries are presented in Fig. 22.

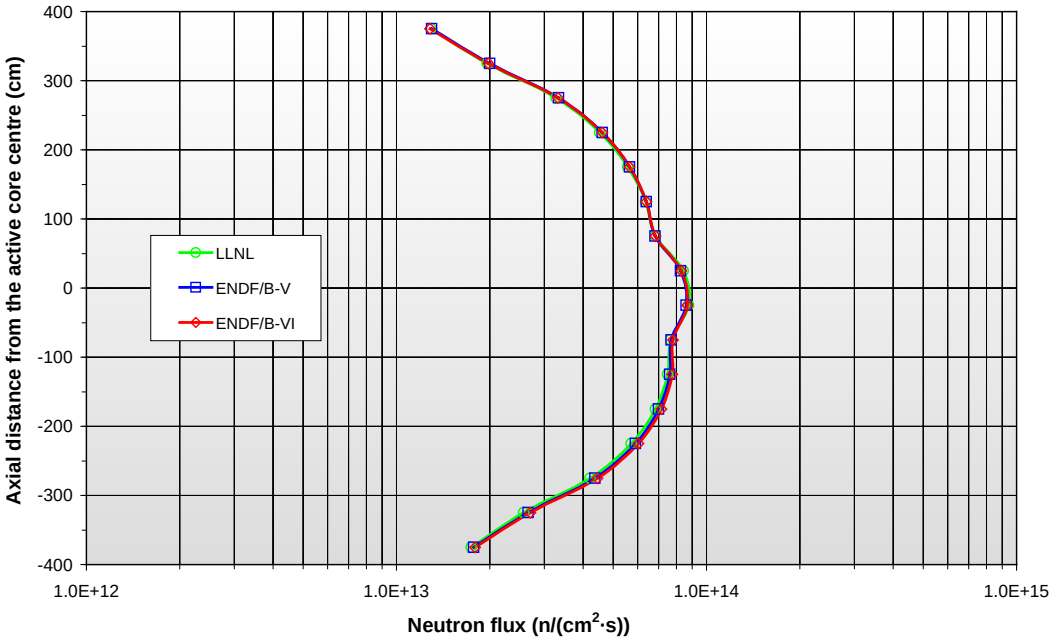

Fig. 22. Thermal neutron fluxes

The achieved results show that there is no significant influence of these analysed data libraries on the modelled neutron fluxes – the average difference along the height of FC is only ~3 % for thermal neutron flux. Similar insignificant differences along the height of FC are observed and for fast (~3 %), for resonance (~4 %) and for total (~2 %) neutron fluxes, but not presented here.

5 Influence of uncertainty of concentration of impurities on neutron activation modelling

In all cases, when performing the neutron activation modelling the activity variation in the axial direction in the structural component being analyzed was assessed and the radionuclides emerging in the activated materials, as well as their radioactivity levels were evaluated at the time just after the irradiation termination (i.e. at the time of RFS), and for several decay (cooling) periods after the irradiation termination, i.e. after the reactor shutdown.

5.1 Graphite rings/sleeves

5.1.1 Case A

In this conservative case (maximal concentration of impurities in GRP-2-125 grade graphite rings/sleeves) the maximal total specific activity of the graphite rings/sleeves is ~$1.2 \cdot 10^7$ Bq/g at the time of reactor shutdown, and, as presented in Fig. 23, axial distribution of the total specific activity is not even.

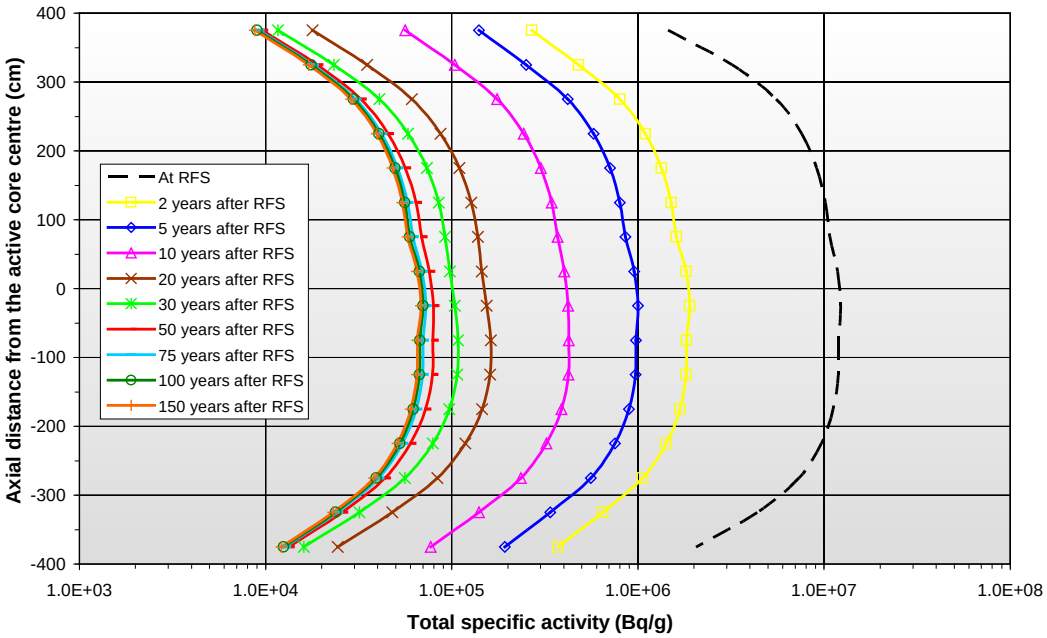

Fig. 23. Axial distribution of the graphite rings/sleeves total specific activity and its variation during 150 years after the reactor final shutdown (Case A)

At RFS, the maximal total specific activity is in the central part of active core where highest thermal neutron flux is observed, while total specific activities of the graphite rings/sleeves in the top and the bottom reflector regions are lower and minimal total specific activity of ~$1.5 \cdot 10^6$ Bq/g is in the top reflector. In other words, the axial distribution as of total specific activity in the graphite rings/sleeves corresponds to the thermal neutron flux distribution in these structures (see Fig. 17). During analysed 150 years after RFS, the maximal total specific activity of active core graphite rings/sleeves decreases to ~$6.8 \cdot 10^4$ Bq/g, while total specific activity of top reflector graphite rings/sleeves decreases to ~$8.8 \cdot 10^3$ Bq/g, see Fig. 23.

The principal radionuclides and their activity variation in the graphite rings/sleeves, which have maximal total specific activity at RFS, are presented in Fig. 17. The most important nuclides (having highest specific activities) during analysed 150 year cooling period in these graphite rings/sleeves are short-lived ^{3}H, ^{55}Fe, and ^{60}Co and long-lived ^{14}C, ^{36}Cl and ^{63}Ni.

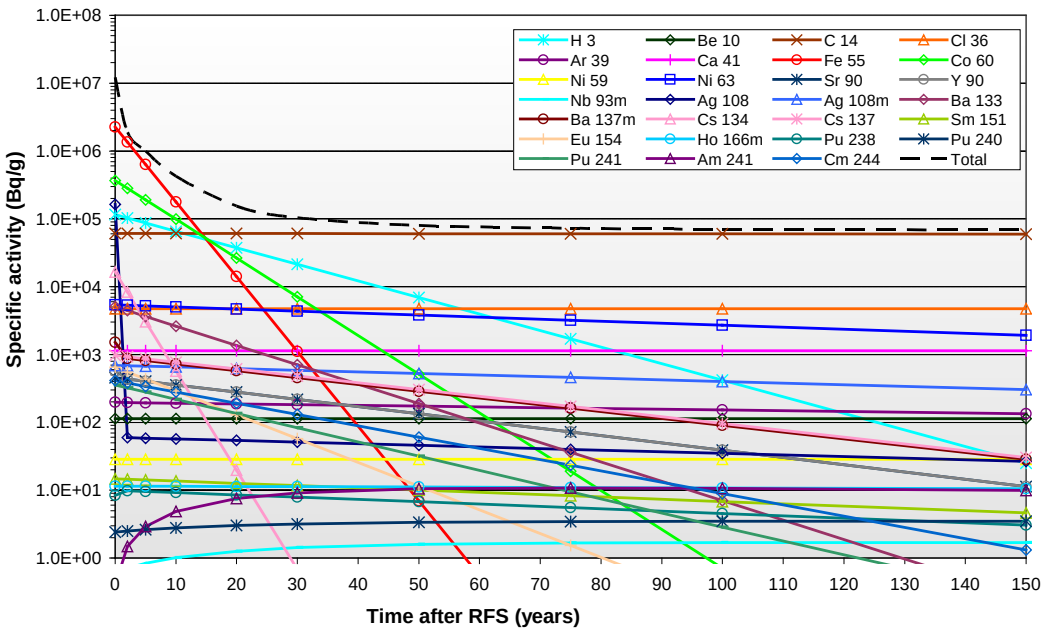

Fig. 24. Principle radionuclides and their activity variation in the graphite rings/sleeves during 150 years after the reactor final shutdown (Case A)

5.1.2 Case B

In this non conservative case (minimal concentration of impurities in GRP-2-125 grade graphite rings/sleeves) the maximal specific activity of graphite rings/sleeves is lower than for

Case A and reaches ~$3.6 \cdot 10^6$ Bq/g at RFS. The axial distribution of the graphite rings/sleeves total specific activity is also not even, as presented in Fig. 18.

At RFS, the maximal total specific activity is in the central part of active core where highest thermal neutron flux is observed, while total specific activities of the graphite rings/sleeves in the top and the bottom reflector regions are lower and minimal total specific activity of ~$5.0 \cdot 10^5$ Bq/g is in the top reflector. In other words, the axial distribution as of total specific activity in the graphite rings/sleeves corresponds to the thermal neutron flux distribution in these structures (see Fig. 17). During analysed 150 years after RFS, the maximal total specific activity of active core graphite rings/sleeves decreases to ~$6.3 \cdot 10^4$ Bq/g, while total specific activity of top reflector graphite rings/sleeves decreases to ~$7.7 \cdot 10^3$ Bq/g (Fig. 25).

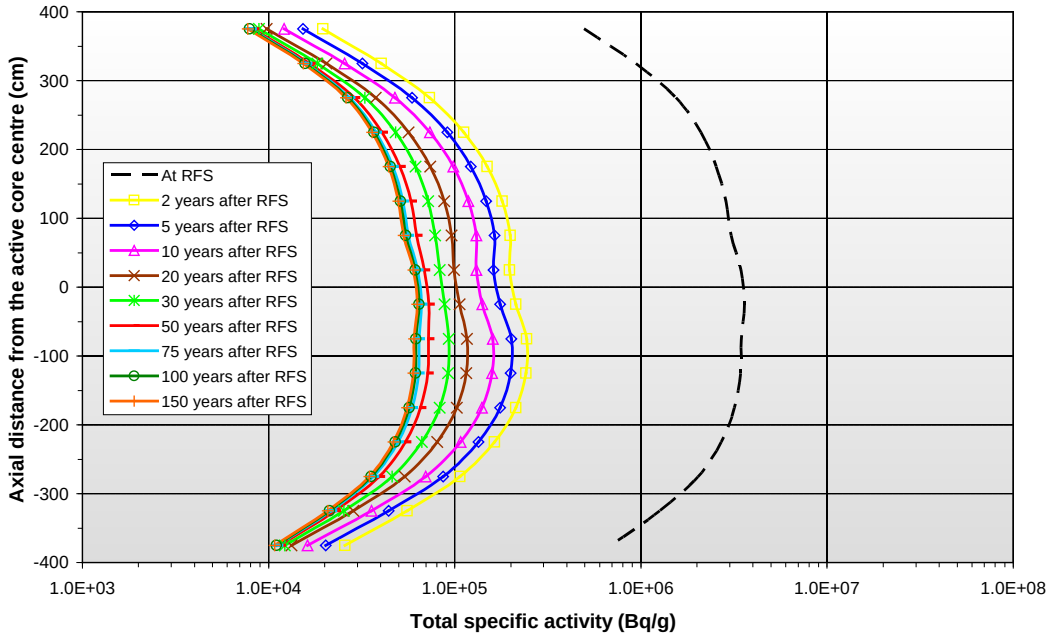

Fig. 25. Axial distribution of the graphite rings/sleeves total specific activity and its variation during 150 years after the reactor final shutdown (Case B)

The principal radionuclides and their activity variation in the graphite rings/sleeves, which have maximal total specific activity at RFS, are presented in Fig. 26.

The most important nuclides (having highest specific activities) during analysed 150 year cooling period in the graphite blocks are the same as for Case A: long-lived ^{14}C, ^{36}Cl and ^{63}Ni and short-lived ^{3}H, ^{55}Fe, and ^{60}Co, however the activity of the last two radionuclides are several ten times lower than in Case A.

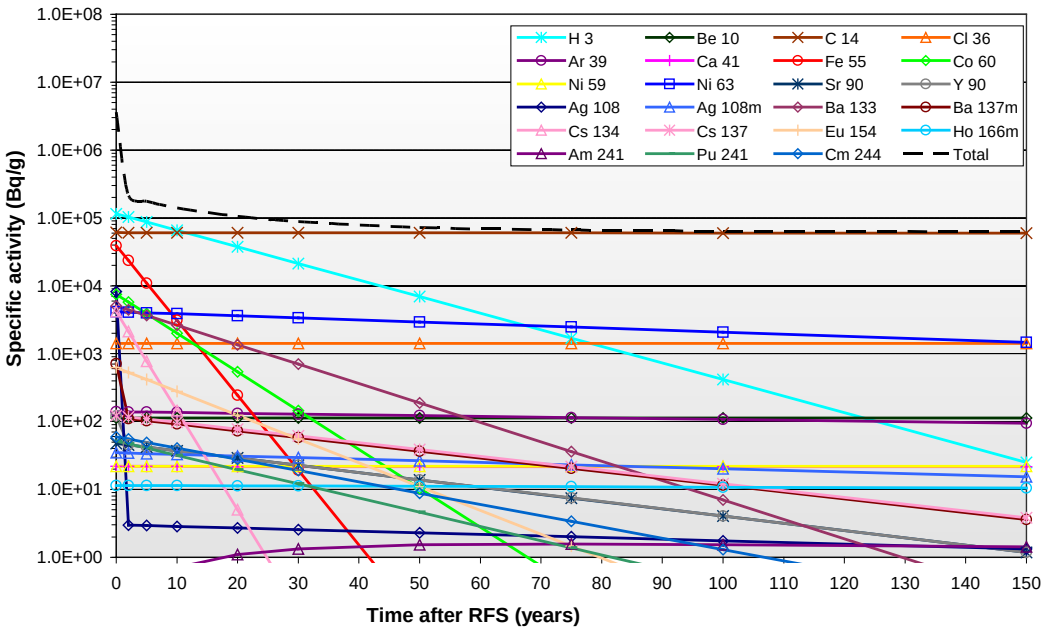

Fig. 26. Principle radionuclides and their activity variation in the graphite rings/sleeves during 150 years after the reactor final shutdown (Case B)

5.1.3 Comparison of the results

After the comparison of axial total specific activity distribution for Case A and Case B it is identified, that differences of initial impurities concentrations have highest impact to the specific activities of active core graphite rings/sleeves while differences of specific activities for the top and the bottom reflector graphite rings/sleeves are lower. This could be explained by the fact that in the active core of the reactor graphite stack, due to the intensive thermal neutron flux and low impurities concentrations a part of impurities (such as Eu and others having large absorption cross-sections) just burns out, while in the regions with considerably lower thermal neutron fluxes (or higher impurities concentrations) they do not burn out completely.

Average (averaged in the axial direction) specific activity of graphite rings/sleeves at the RFS reaches $8.2 \cdot 10^6$ Bq/g and $2.3 \cdot 10^6$ Bq/g for Case A and Case B respectively, so at RFS these activities differ ~3.5 times for maximal and minimal initial impurities concentrations cases. 2 years after RFS when very short-lived radionuclides decay this difference increases to ~9 times

and monotonically decreases to ~1.2 time during 30 years of cooling and for the rest cooling time up to 150 years practically remains constant and is ~1.1 time.

Such a difference for the first ~20 cooling years is determined by the differences of ^{55}Fe and ^{60}Co activities due to the different initial concentrations of Fe and Co impurities. For the Case A namely ^{55}Fe and ^{60}Co radionuclides comprise highest parts of the total specific activity for the first ~20 cooling years. However, due to the radioactive decay their activities rapidly decrease and after ~30 years of cooling their contribution became insignificant and ^{14}C specific activity starts to dominate.

For the Case B ^{55}Fe and ^{60}Co still are one of the most active radionuclides at RFS but their activities do not considerably influence the total specific activity which is determined by ^{3}H and ^{14}C. For both modelling cases during 30–150 cooling years the total specific activity is determined by the activity of ^{14}C which is activation product of graphite raw material (carbon), so the activities of ^{14}C do not differ much as carbon concentration in the graphite for both cases is almost identical.

5.2 Graphite blocks

5.2.1 Case A

In this conservative case (maximal concentration of impurities in GR-280 grade graphite) the total specific activities of the graphite blocks within the top reflector, the active zone and the bottom reflector are quite even distributed comprising $(1.1–1.4)\cdot10^{8}$ Bq/g at the time of reactor shutdown, see Fig. 20. Only after longer cooling time (time following the reactor final shutdown) not even distribution of total specific activity is observed and starts to correspond to the distribution of the thermal neutron flux (see Fig. 16) where the maximal activity is observed in the centre graphite blocks of the active core, whereas the minimal – in the top and bottom reflector blocks.

This corresponds to the fact that in the active core of the reactor graphite stack, due to the intensive thermal neutron flux, a part of impurities (such as Li, Eu and others having large absorption cross-sections) burns out and activities of their activation products, which have short half-lives, already decreased by the radioactive decay. While in the regions of the top and the bottom reflectors, where thermal neutron fluxes are considerably lower, mentioned

impurities burns out not so quickly and this determines higher activities of their activation products at the time of the reactor final shutdown. This can be seen in the Fig. 27, where axial variation of the graphite blocks total specific activity during 150 years after RFS is presented; during cooling time the short-lived activation products of "burnable" impurities in the reflector regions quickly decay and with longer cooling times the axial distribution of total specific activity starts stronger correlate to the thermal neutrons distribution profile in the graphite column.

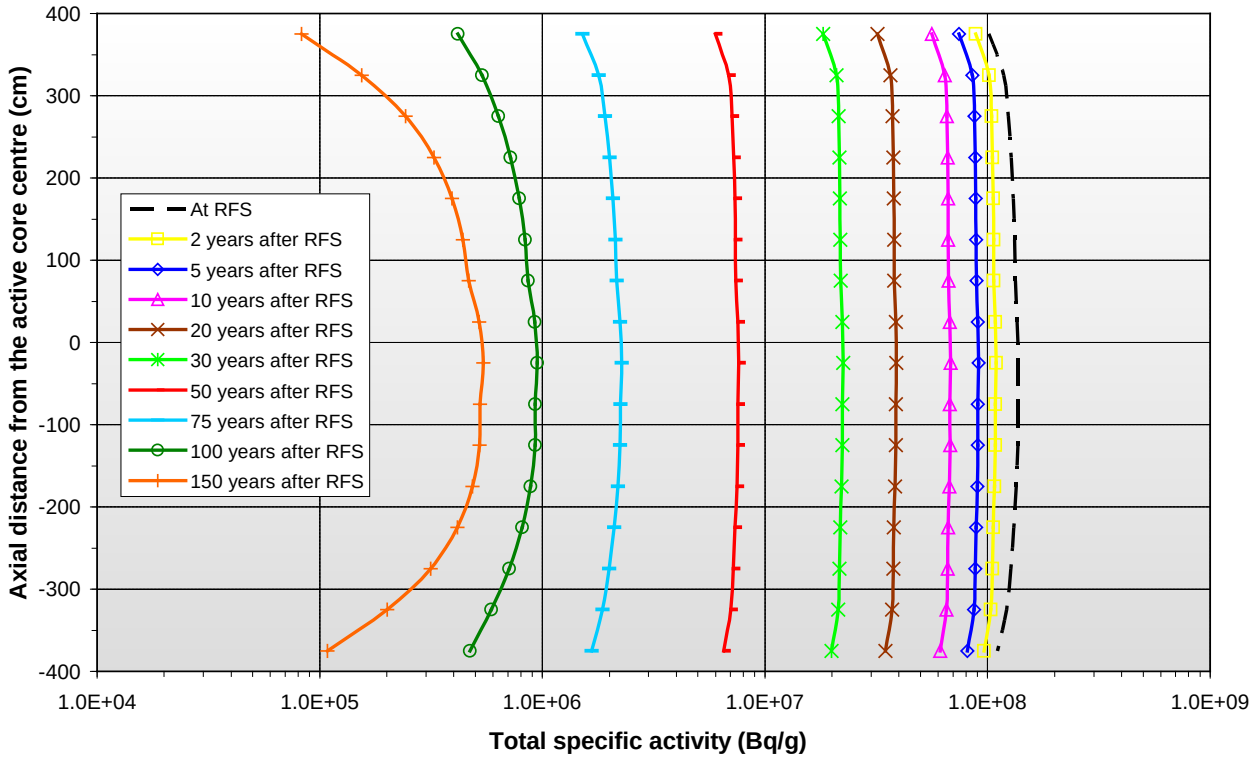

Fig. 27. Axial distribution of the graphite blocks total specific activity and its variation during 150 years after the reactor final shutdown (Case A)

The principal radionuclides and their activity variation in the graphite blocks of the central part of the graphite column (where maximal specific activity is observed at RFS) are presented in Fig. 28.

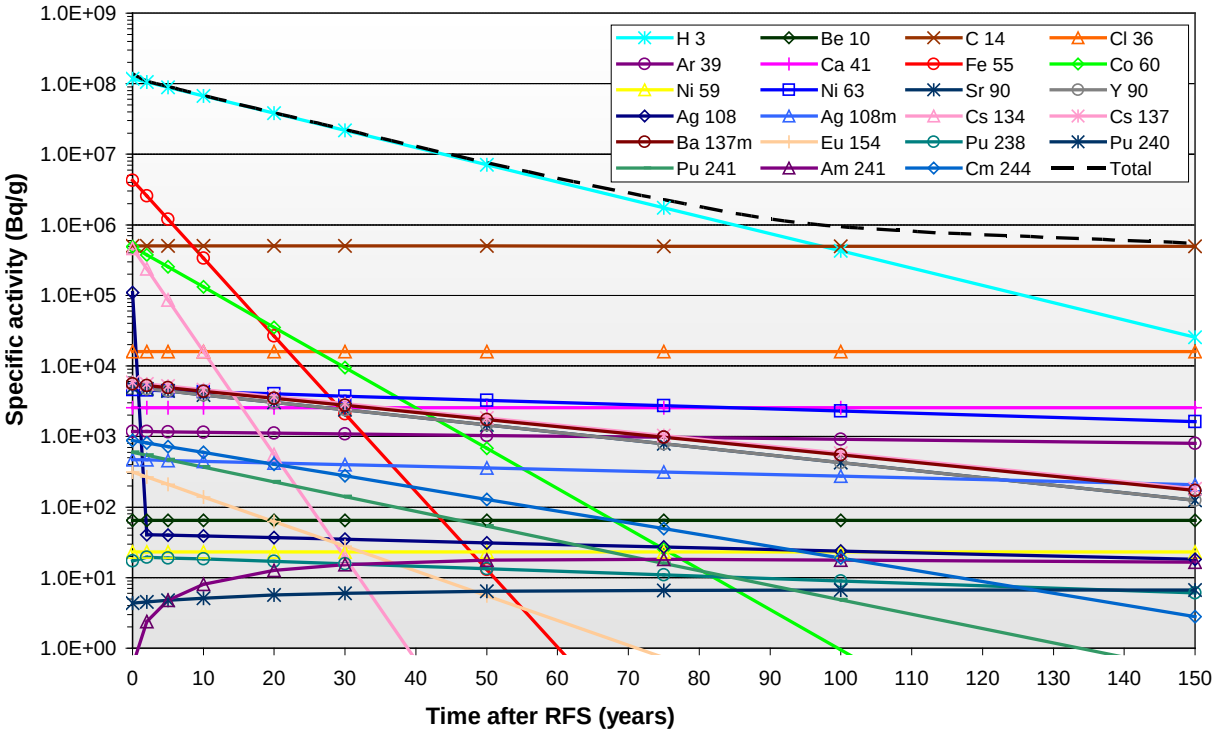

Fig. 28. Principle radionuclides and their activity variation in the graphite blocks during 150 years after the reactor final shutdown (Case A)

The most important nuclides (having highest specific activities) during 150 year cooling period in the graphite blocks are as follows: ^{55}Fe, ^{60}Co, ^{3}H, ^{14}C, ^{36}Cl, ^{63}Ni, ^{41}Ca, and ^{39}Ar. In this case the total specific activity is determined by ^{3}H and only ~100 years later ^{14}C starts to dominate.

5.2.2 Case B

In this non conservative case (minimal concentration of impurities in GR-280 grade graphite blocks) the distribution of the total specific activity along the graphite blocks column is not even, as presented in Fig. 29. At RFS, the maximal specific activities are observed in the top and the bottom reflectors blocks, where thermal neutron flux is lowest (see Fig. 16).

The maximal total specific activity of the bottom reflector graphite blocks is ~$1.4 \cdot 10^{6}$ Bq/g while for active core graphite blocks it is ~$7.0 \cdot 10^{5}$ Bq/g at RFS. After several decades the maximal total specific activity is observed in the graphite blocks of the active core central part where thermal neutron fluxes are highest. This is determined by the already mentioned burnup process of the initial impurities (mainly Eu in this particular case).

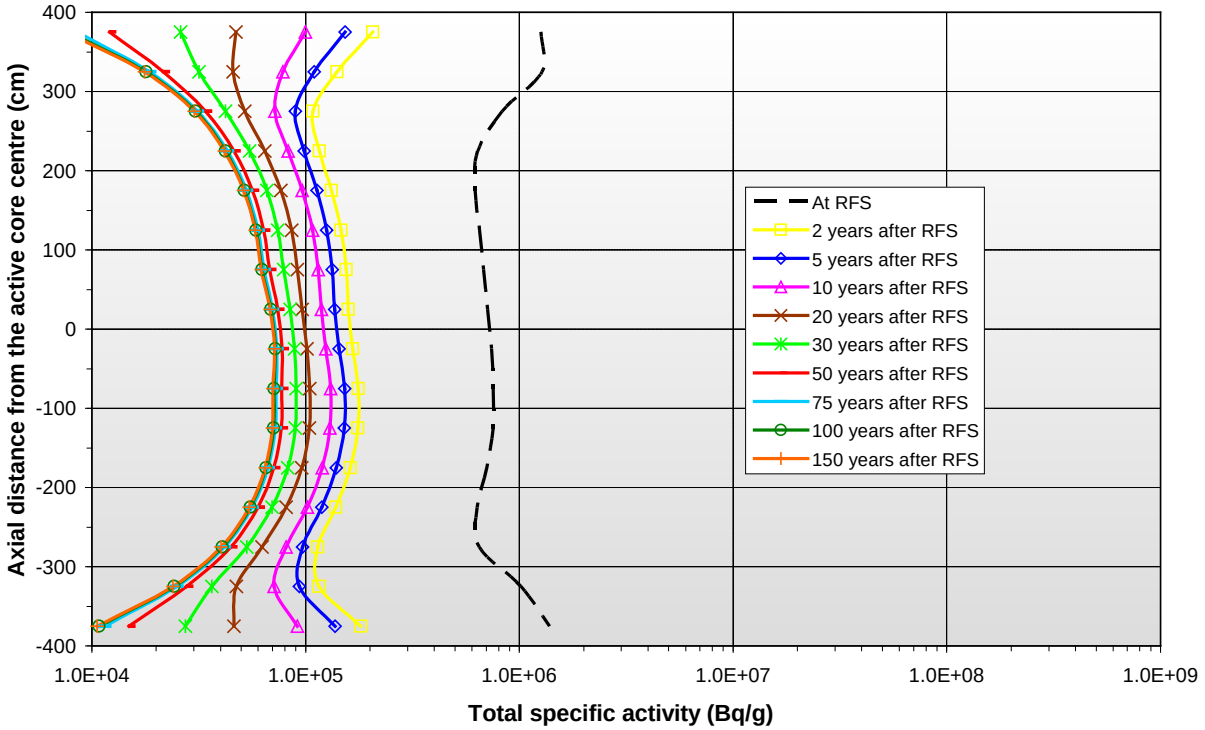

Fig. 29. Axial distribution of the graphite blocks total specific activity and its variation during 150 years after the reactor final shutdown (Case B)

Principle radionuclides and their activity variations in the graphite blocks of bottom reflector (375 cm below the centre of the active core where maximal total specific activity at the RFS is observed) and active core graphite blocks (175 cm above the centre of the active core where minimal total specific activity at the RFS is observed) are presented in Fig. 30 and Fig. 31 respectively. These results clearly indicate that Eu impurity is burned out in the central part of active core and activities of Eu isotopes are lower than in the bottom reflector.

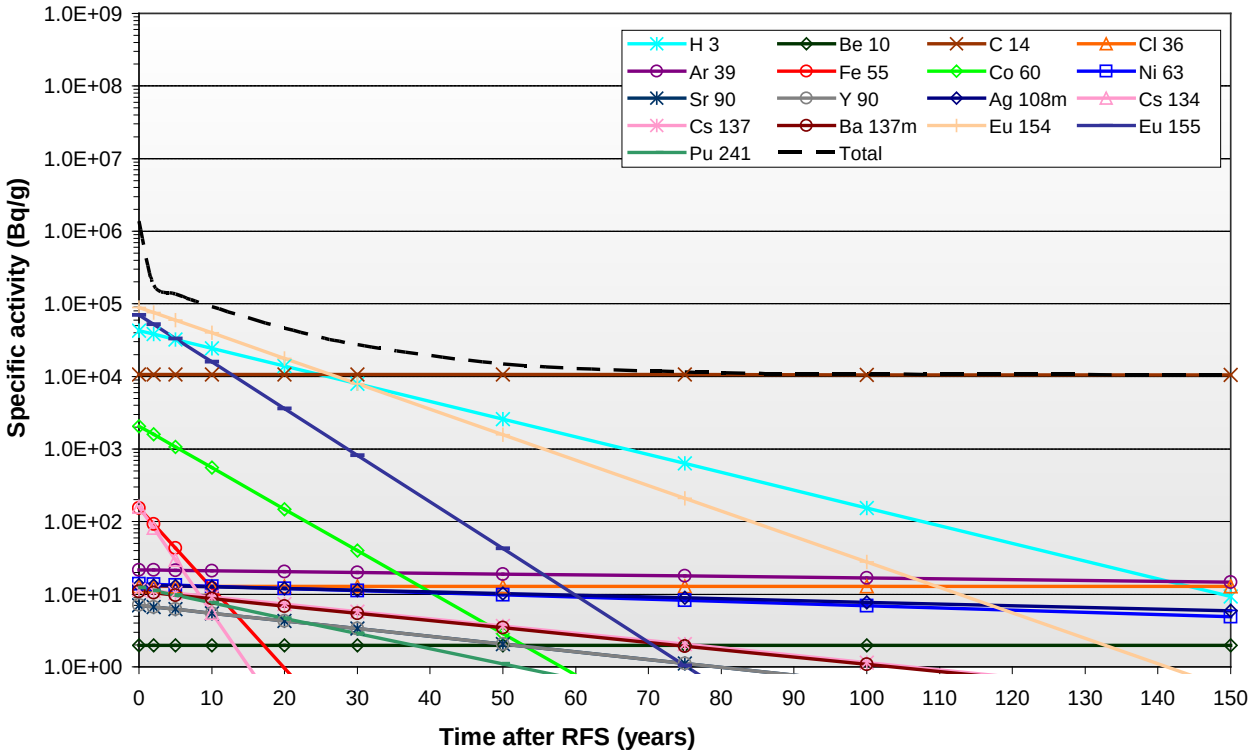

Fig. 30. Principle radionuclides and their activity variation in the graphite blocks (375 cm below the centre of the active core) during 150 years after the reactor final shutdown (Case B)

The most important nuclides (having highest specific activities) for this non conservative case, similar to the conservative Case A, are ^{3}H, ^{55}Fe, ^{60}Co (short-lived) and long-lived ^{14}C in the active core graphite blocks. However, contrary for the Case A, tritium determines total specific activity for relatively short time – after 10 years ^{14}C starts to dominate. For graphite blocks of the top and the bottom reflectors total specific activity is determined by short-lived ^{154}Eu, ^{155}Eu and ^{3}H, and only later (after ~30 years of cooling) total specific activity is determined by ^{14}C.

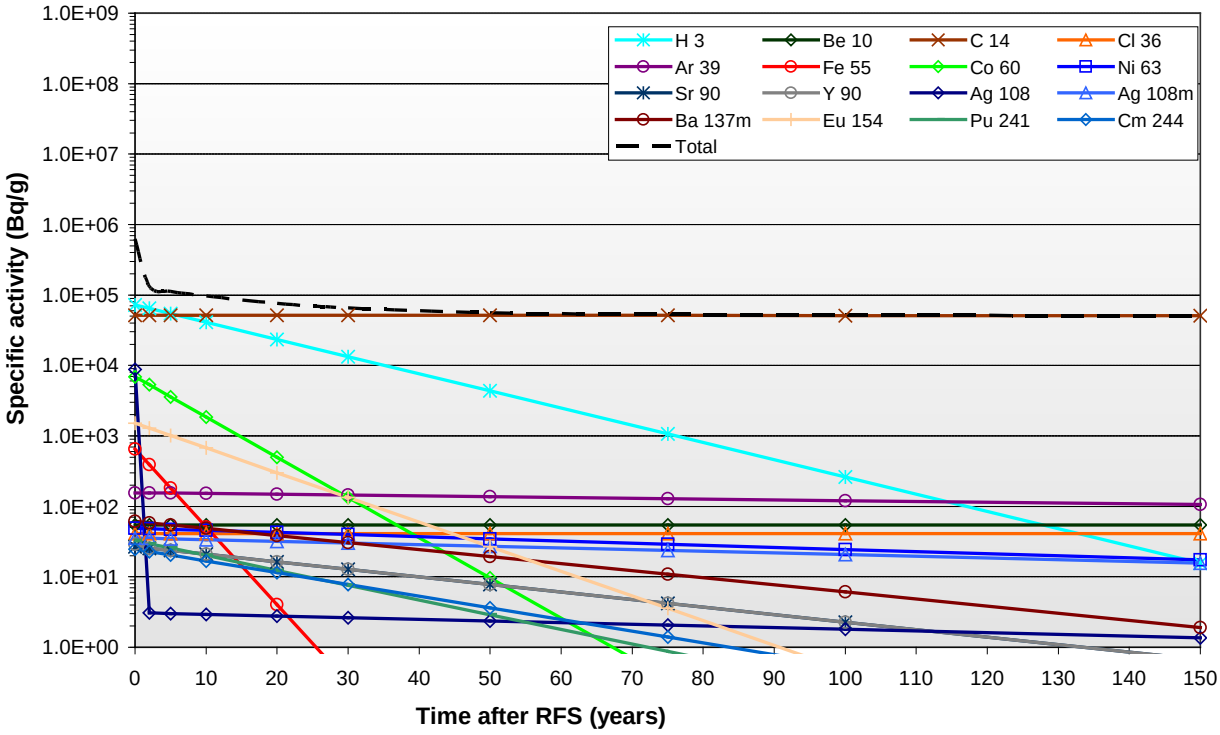

Fig. 31. Main radionuclides and their activity variation in the graphite blocks (175 cm above the centre of the active core) during 150 years after the RFS (Case B)

5.2.3 Comparison of the results

Comparison of graphite blocks total specific activity axial distribution for Case A and Case B shows that differences of initial impurities have impact not only to the total specific activity but also to its axial distribution profile. This, similarly to the graphite rings/sleeves cases, could be explained by the fact that in the active core of the reactor graphite stack, due to the intensive thermal neutron flux and low impurities concentrations a part of impurities (mainly Eu in this particular case) just burns out, while in the regions with considerably lower thermal neutron fluxes (or higher impurities concentrations) this process asserts not so significantly.

Average (averaged in the axial direction) specific activity of the graphite blocks column at the RFS is $1.3 \cdot 10^8$ Bq/g and $8.3 \cdot 10^5$ Bq/g for Case A and Case B, respectively. After 150 cooling years the activities decrease to ~$3.6 \cdot 10^5$ Bq/g and ~$4.6 \cdot 10^4$ Bq/g. So at RFS the average total specific activities differ more than 10^2 times for maximal and minimal initial impurities concentrations cases and after 150 cooling years the difference decreases to ~10 times.

This difference is determined mostly by the high differences of initial concentrations of such impurities as Li, Fe and Co (more than 10^3 times for Li and Fe and about 50 times for Co). For the Case A their activation products, namely ^{3}H (for the first ~100 cooling years) and less significantly ^{55}Fe and ^{60}Co, (for the first ~10 cooling years) determines total specific activity of the active core graphite blocks. While for the Case B only ^{3}H considerably influences total specific activity from mentioned radionuclides, however its activity is still more than 10^3 times lower than in Case A. For cooling period of 100–150 years the total specific activity is determined by the specific activity of ^{14}C in both modelling cases. ^{14}C arises as activation product of graphite raw material (carbon) and as activation product of nitrogen impurity; however nitrogen impurity concentration in modelling Case A is more than 10^2 times higher than in modelling Case B and thus the activity of ^{14}C is considerably higher in Case A.

5.3 Discussion

The average total specific activities (averaged over the whole height of the graphite stack) in the analyzed RBMK-1500 reactor graphite components during 150 cooling years after the reactor final shutdown are presented in Fig. 32.

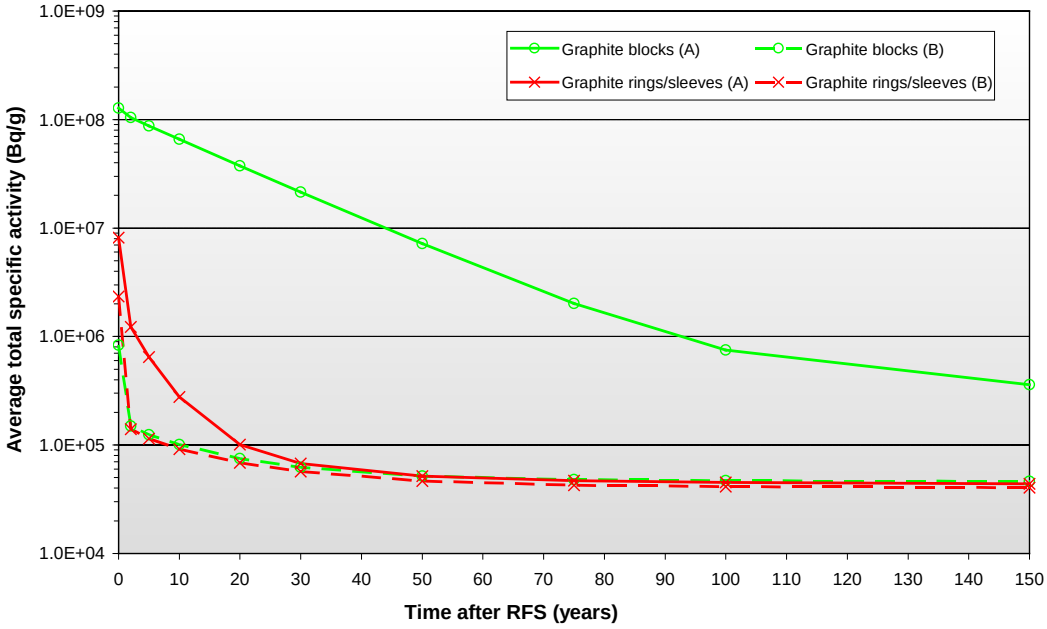

Fig. 32. Variation of the average total specific activity of the graphite components of Ignalina NPP Unit 1 reactor during 150 years after the reactor final shutdown

During 150 years cooling time the induced activities in the graphite structural components being analyzed decrease with different pattern: from several ten times for the graphite blocks and rings/sleeves for minimal impurities concentrations cases to several hundred times for the graphite blocks and rings/sleeves for maximal impurities concentrations cases.

Fig. 32 also show that the influence of different initial materials compositions for the graphite components activities vary with time. Thus, in order to assess the potential impact of the initial impurities concentrations on the induced activities in the particular reactor component at certain time after RFS, the time period passed from the reactor shutdown should also be accounted. Furthermore, comparing the induced activities in the graphite rings/sleeves and blocks the later have higher activity at the time of RFS and during the analyzed cooling period for maximal impurities concentration cases. Similar situation is and for minimal impurities concentration cases, however at the time of RFS graphite rings/sleeves have slightly higher activity due to the presence of more very short-lived radionuclides compared to the graphite blocks.

6 Influence of nitrogen activation on ^{14}C concentration

The activity of ^{14}C in the graphite samples of the RBMK reactor core has been measured by β spectrometry technique [19] and calculated by MCNPX coupled with CINDER after 11.6 years of irradiation as described in 2.4.1. The measured values of ^{14}C activity are considerably bigger than calculated values of ^{14}C activity in the graphite constructions of the RBMK reactor as it is presented in Table 9.

Table 9. Simulated activity of ^{14}C in the RBMK graphite constructions and experimental values of activity of ^{14}C in graphite samples (Gr.13, Gr.14, Gr.16, Gr.18).

A (^{14}C), kBq/g		**Graphite construction**		
	Stack	**Sleeve (Gr.13, Gr.14)**	**Top reflector (Gr.18)**	**Bottom reflector (Gr.16)**
Modelled values from $^{13}C(n,\gamma)^{14}C$ reaction for RBMK-1500	42.7	35.2	7.4	7.4
Experimental values for RBMK-1500		130±20	13±4	24±6
Modelled values from all reactions for RBMK-1000 [25]	185		≤37	≤37

This can be explained by the fact that ^{14}C is also produced in $^{14}N(n,p)^{14}C$ reaction, which was not taken into account by MCNPX calculations. Nitrogen is used to flush the graphite stack of the RBMK reactors therefore we expect that its activation reaction mostly occurs on the surface (30 nm according to ref. [26]) of graphite where non-negligible amount of ^{14}N from cooling gas of the core cooling gas circuit can be accumulated. The impurities of ^{14}N in the graphite stack comprise 0.5 – 70 ppm as reported in [7]. Taken into account this concentration the amount of ^{14}C produced in $^{14}N(n,p)^{14}C$ was calculated by MCNPX in a similar way as in the case of $^{12}C(n,\gamma)^{13}C$, $^{13}C(n,\gamma)^{14}C$ considering appropriate macroscopic cross-sections. The lowest ^{14}N concentration range corresponds to an increase of ^{14}C activity by 18%, and the highest range – an increase even 25 times. As one can see the experimental values of ^{14}C activity are 3.7 times higher compared with the model (see Table 9). This corresponds to 7.6÷2.0 ppm impurity of ^{14}N according to [7].

Simulated values for the RBMK-1000 reactor [25] presented in Table 3 are higher than our calculated values for the RBMK-1500 reactor by 4.3 times. Our modelled and experimental values are to some extent in agreement with data published in [25] taking into account that one half of the calculated activity in [25] is caused by ^{14}N impurity activation in the reactor core. In [25] the specific activity of ^{14}C in the graphite stack, graphite side reflectors and graphite extracting bushings (sleeves) after final shut-down of the reactor is estimated in the context of incineration of graphite as a combustible radioactive waste. The RBMK-1000 reactor is very similar to the RBMK-1500 one. The major difference is the design power and correspondingly, neutron flux and activation of reactor constructions. Moreover, the power of the RBMK-1500 reactors at the Ignalina NPP was reduced from 4800 MW to 4200 MW for safety reasons after the Chernobyl accident; therefore the real difference could be even smaller.

7 Influence of radionuclide activity on management of graphite irradiated in RBMK-1500 reactor

For analysis of influence of radionuclide activity on management of graphite irradiated in RBMK-1500 reactor calculations with validated model (see 3.1.3) were used.

Despite the fact that difference of radionuclide specific activities due to impurity activation in the graphite sleeve and stack constructions is not considerable (less than 15%) for most of them, but small difference can become crucial estimating the radionuclides which are on the clearance levels limit; for instance, concentration of ^{239}Pu in the stack is below the clearance level but in the sleeve its 22% higher activity is on the limit (see also Fig. 33 for more details).

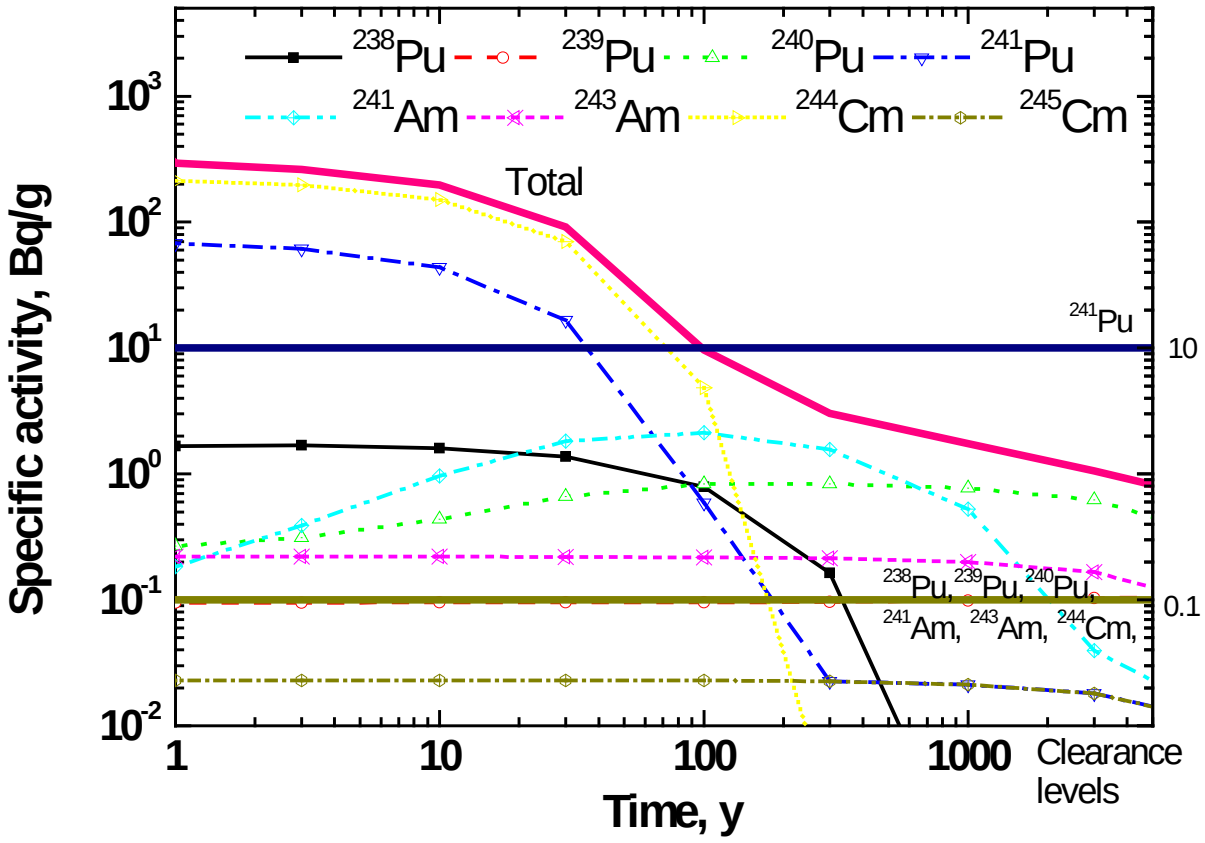

Fig. 33. Specific activities of actinides as a function of cooling time in the graphite sleeve (the clearance lines for actinides on the right in Bq/g for listed nuclides)

The specific activities of other radionuclides which exceed or are close to their clearance level (according to Lithuanian norms) as a function of the cooling time are shown in Fig. 34. The highlighted lines and the notes on right of the lines indicate clearance levels for individual radionu-clides. The total activity decreases sharply after shutdown of the reactor because of the decay of short-lived nuclides, while after 10 years of cooling it changes very slowly for a long time.

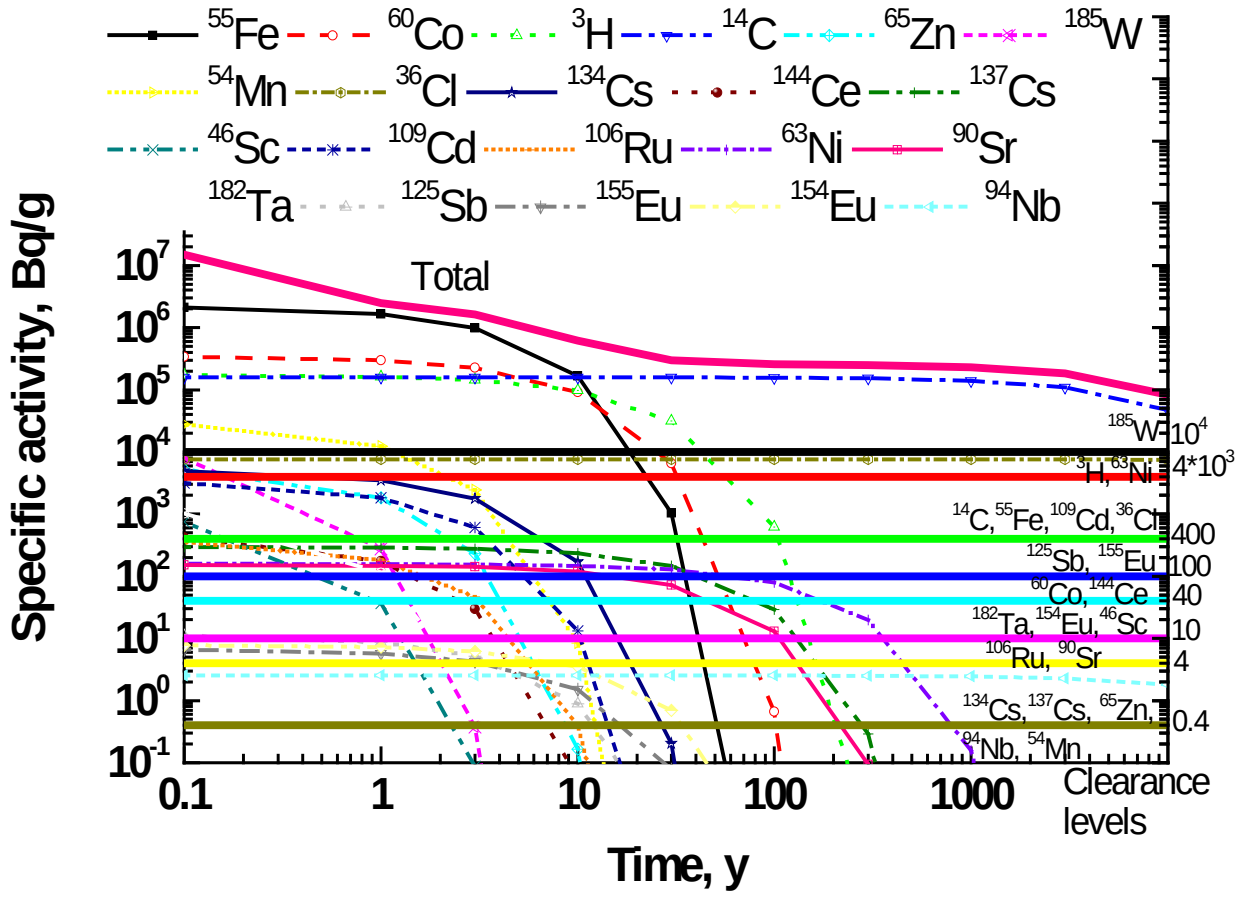

Fig. 34. Specific activities of radionuclide as a function of cooling time in the graphite sleeve (the clearance lines on the right in Bq/g for listed nuclides)

^{14}C and ^{3}H compose the long-term radiotoxicity of graphite waste, while ^{55}Fe, ^{60}Co, ^{65}Zn, ^{54}Mn, ^{36}Cl are important for dismantling on the site. ^{109}Cd, ^{125}Sb, $^{154\text{-}155}$Eu do not exceed the clearance levels. By comparing our results based on new impurity concentrations with the previous calculations [7], we obtain higher values for ^{55}Fe, ^{36}Cl and lower values for ^{14}C

concentrations, the ^{60}Co and ^{3}H concentrations are quite similar. ^{14}C is very important for selection of the best option for waste management and a lower value of the activity is more favourable from the point of view of long-term disposal.

The specific activities of actinides as a function of the cooling time are presented in Fig. 33. ^{244}Cm and ^{241}Pu dominate at the first 100 years, afterwards until 1000 years dominates ^{241}Am. We have obtained higher actinide concentration than one in the previous work [7]. New values of actinide concentration exceed unconditional clearance levels and can create an additional problem for waste management.

8 Validation of activity calculation model

For validation of results calculated by simulation of activation of the reactor graphite constructions specific activity of alpha emitters in irradiated RBMK-1500 graphite sleeve have been measured by alpha-spectrometer with PIPS detectors CANBERRA. A limit of detection of 0.03 Bq/kg was calculated for alpha-spectrometric determination of actinides which is equivalent to an absolute detection limit of 0.0004 Bq with a counting time 100,000 s and 50% chemical recovery.

The measured values of ^{238}Pu, $^{239+240}$Pu, ^{241}Am, ^{242}Cm, and ^{242}Cm activities in irradiated RBMK-1500 graphite sleeve samples (see Fig. 12) are presented in Table 10.

Table 10. Experimental values of activity of actinides in graphite sleeve samples.

Nuclide	^{238}Pu	$^{239+240}$Pu	^{241}Am	^{242}Cm	^{242}Cm
Specific activity	400±70	70±20	120±50	90±30	(1.1±0.2)10^{4}

Results of comparison of ratios of simulated values of the actinides activity to measured ones are shown in Fig. 35 and Fig. 36. The medial dotted line corresponds to the central value of the measured ratio, and the edge dotted lines correspond to limit values of the errors.

As can be seen from Fig. 35 the ratio of simulated and measured activities for Pu isotopes coincides, taking into account measurement errors, after 15 years of activation of the graphite in the reactor. The value of simulated ration goes down after 20 years when the reactor is shut down and amount of ^{238}Pu decreases significantly due to end of its generation from ^{238}Np.

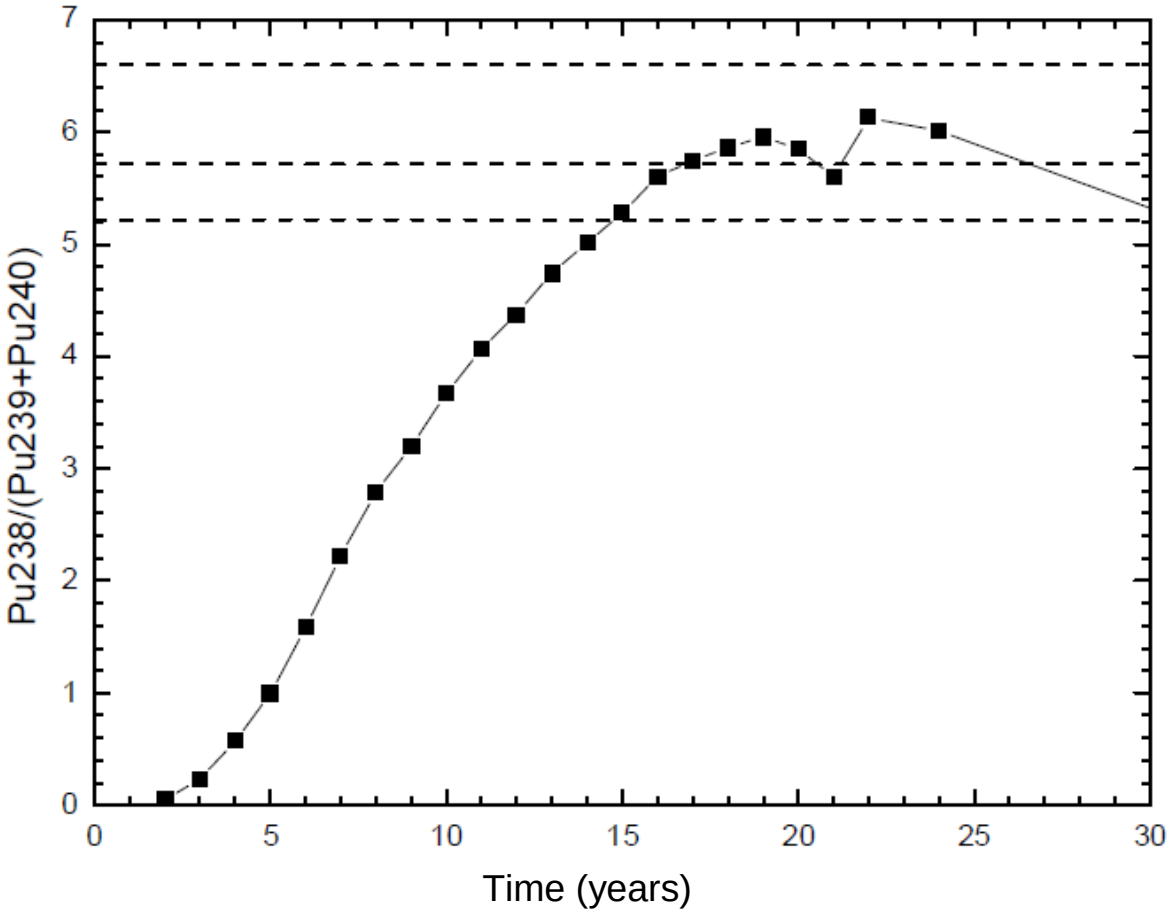

Fig. 35. Time dependence of the ratio of simulated specific activities for Pu isotopes and confidence intervals of measured values of the ratio

Fig. 36 shows time dependence of the simulated ratio of specific activities of 243+244Cm and 241Am. The simulated and measured values of the ratio coincide at two time moments: after 12 years of irradiation in the reactor and after the reactor RFS. The ratio of specific activities of 243+244Cm and 241Am grows when the reactor is in operation and reaches the maximum value at RFS. After RFS the ratio sharply decreases due to generation of 241Am from beta decay of 241Pu.

The simulated value of the ratio and measured one become equal after about 5 years from RFS at the time when the measurement has really been done. This coincidence justifies applicability of created computer model for simulation of isotope generation in the irradiated RBMK-1500 graphite.

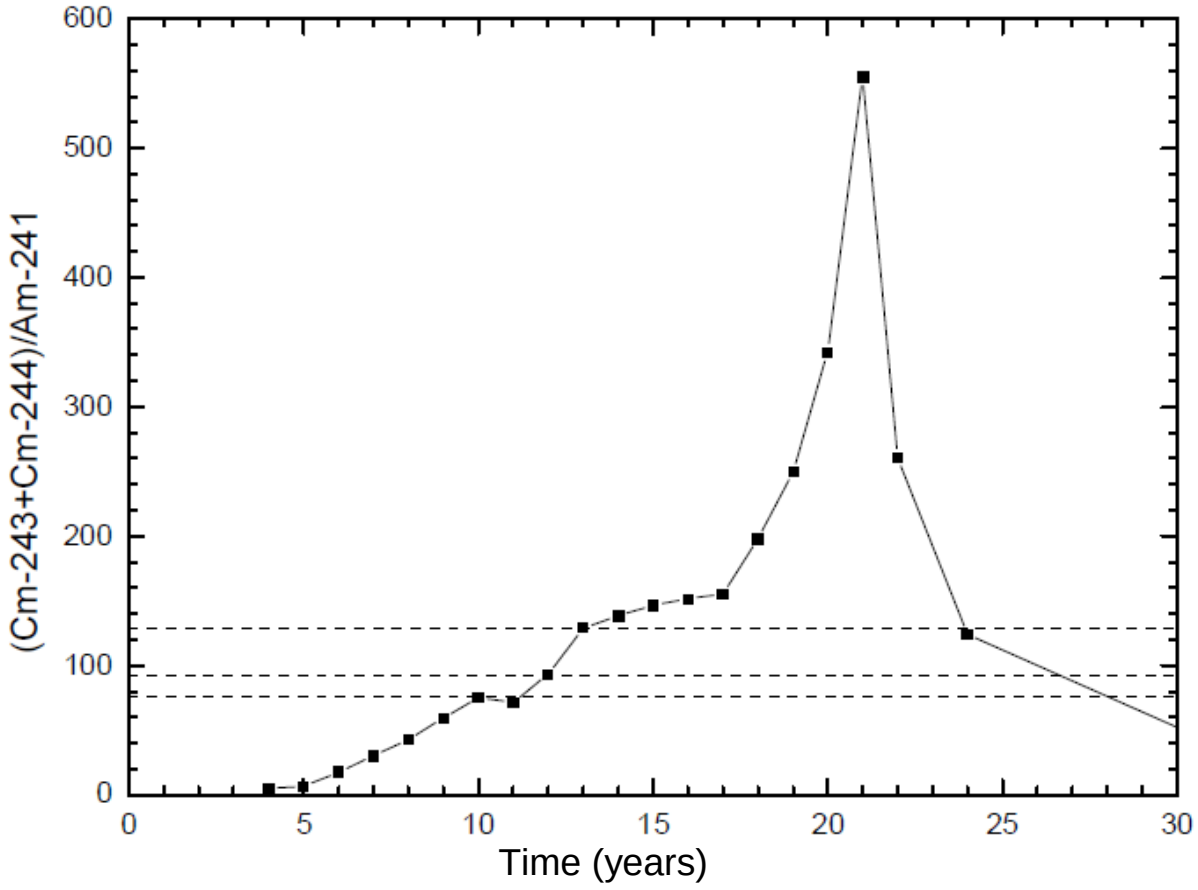

Fig. 36. Time dependence of the ratio of simulated specific activities for Cm and Am isotopes as well as confidence intervals of measured values of the ratio

9 Summary and conclusions

The performed evaluation of the neutron flux distribution in the central part of the RBMK-1500 reactor core (plateau) using the developed three dimensional numerical model of the RBMK-1500 reactor core, neutron activation analysis of the reactor graphite constructions performed basing on the obtained neutron flux modelling results taking into account IRMS, mass, alpha and beta spectrometric measurements allows to summarise that:

- for precise evaluation of the neutron fluence in any position of the graphite stack or other graphite constructions in the graphite moderated reactor and for determination of ^{14}C activity in carbonaceous materials uncertainties of microscopic cross sections for

reactions $^{12}C(n,\gamma)^{13}C$, $^{13}C(n,\gamma)^{14}C$, $^{13}C(n,\gamma)^{10}Be$, and $^{14}N(n,p)^{14}C$ have to be taken into account;

- a new general method based on combination of the results ($\delta^{13}C$ values) of mass spectrometry and the results of computer modelling of the integral neutron flux in the reactor core can be used for calibration of computer modelling to escape model input data uncertainties;
- ICP-MS is a promising technique for determination of concentration of graphite minor impurities as it is a rapid and a relatively cheap method;
- the most important elements for and evaluation of short- and long-lived activation products in the irradiated RBMK-1500 graphite by simulation of activation were measured with the accuracy sufficient for the characterization of radioactive waste;
- neither fuel type or its burnup nor the analysed data libraries have critical influence on the determined neutron flux intensity and energetic distribution;
- for the conservative modelling case, the specific activity of the graphite blocks is in the order 10^8 Bq/g of magnitude just after the reactor final shutdown and is higher than that of the graphite rings/sleeves (less than 10^7 Bq/g) and stays higher during all analyzed cooling time, because the graphite blocks are exposed to the higher thermal neutron fluxes and have higher initial concentrations of impurities (Co, Li, N, etc.);
- for the non conservative case, specific activity of graphite blocks is several times lower than for conservative case, while specific activity of graphite rings/sleeves for both cases differs not significant (except ~10 years after RFS), as this activity is mostly determined by activation of graphite raw material (carbon) and used assumption on the absences of nitrogen impurity for this grade graphite in both cases;
- achieved results confirmed that the radionuclides ^{3}H, ^{55}Fe, ^{60}Co (short-lived) and ^{14}C, ^{36}Cl, ^{63}Ni (long-lived) have the highest activities in the graphite components, thus a proper determination of the initial impurities (Fe, Co, Li, N, Cl and Ni, which give rise to the mentioned radionuclides) concentrations is important, as they can vary in the wide range from several ten to several thousand times. The proper determination of initial U concentration is also needed for a proper determination of its fission products;

- values of actinide concentration exceed unconditional clearance levels and can create an additional problem for irradiated graphite waste management.

10 References

1. Almenas, K.; Kaliatka, A.; Uspuras, E. 1998. *Ignalina RBMK-1500: A source book, 2nd ed.* Kaunas, Lithuania: Lithuanian Energy Institute.
2. IAEA 1998. Radiological Characterization of Shut Down Nuclear Reactors for Decommissioning Purposes. *Technical Report Series*: 389. Vienna, Austria: International Atomic Energy Agency.
3. Bylkin, B. K.; Davydova, G. B.; Krayushkin, A. V.; Shaposhnikov, V. A. 2004. Computational Estimates of the Radiation Characteristics of Irradiated Graphite after Final Shutdown of a Nuclear Power Plant with an RBMK Reactors. *At. Energ*. 96(6): 411–416.
4. Bylkin, B. K.; et. al. 2001. Induced Radioactivity and Waste Classification of Reactor Zone Components of the Chernobyl Nuclear Power Plant Unit 1 after Final Shutdown. *Nucl. Technology* 136: 76–88.
5. Virgilev Yu. S. Impurities in and Serviceability of Reactor Graphite. 1998. *At. Energ*. 84(1): 6–13.
6. Bushuev, A. V.; Zubarev, V. N.; Proshin, I. M. 2002. Impurity Composition and Content in Graphite from Commercial Reactors. *Atomic Energy* 92(4): 331–335.
7. Ancius, D.; et. al. 2005. Evaluation of the Activity of Irradiated Graphite in the Ignalina Nuclear Power Plant RBMK-1500 Reactor. *Nukleonika* 50(3): 113−120.
8. Puzas, A.; Remeikis, V.; Ežerinskis, Z.; Serapinas, P.; Plukis, A.; Duškesas, G. 2010. Mass Spectrometric Determination of Impurities in Reactor Core Graphite for Radioactive Waste Composition Modelling. *Lith. J. Phys*. 50(4): 445–449.
9. Jegyzokonyv, M.; Mauerhofer, E. 2010. RBMK Impurities. Results of the PGAA Measurements. *Report on Prompt Gamma Analysis Measurements*. Budapest, Hungary:

Institute of Isotopes of Hungarian Academy of Sciences (private communication from Revay Z. to Vulpius D. on 20 Dec. 2010).

10. INPP 2002. Ignalina NPP Unit 2 Safety Analysis Report. *Document PTOab2–0345–5112V1*. Visaginas, Lithuania: Ignalina NPP.
11. Narkūnas, E.; Šmaižys, A.; Poškas P. 2009. Numerical modelling of neutron activation processes in reactor RBMK-1500 structural elements. 3. Modelling of neutron activation processes in fuel channels employing modelled neutron fluxes. *Power Engineering* 55(4): 200–208 (in Lithuanian).
12. Remeikis, V.; Plukis, A.; Plukienė, R.; Garbaras, A.; Barisevičiūtė, R.; Gudelis, A.; Gvozdaitė, R.; Duškesas, G.; Juodis, L. 2010. Method based on isotope ratio mass spectrometry for evaluation of carbon activation in the reactor graphite. *Nucl. Eng. Des.* 240: 2697-2703.
13. Wilson, W. B.; Cowell, S. T.; England, T. R.; Hayes, A. C.; Moller, P. 2007. A Manual for CINDER'90 Version 07.4 Codes and Data. *Report LA-UR-07-8412*. New Mexico, USA: Los Alamos Nat. Lab.
14. Gardner, M. A.; Howerton, R. J. 1978. ACTL - Evaluated Neutron Activation Cross Section Library - Evaluation Techniques and Reaction Index. *Package DLC-69/ACTL* (*UCRL-50400 vol. 18, Lawrence Livermore Lab.*). Oak Ridge, USA: Radiation Shielding Information Center.
15. Plukis, A.; Plukienė, R.; Puzas, A.; Remeikis, V.; Duškesas, G. 2010. Nuclear data needs for reactor graphite radiological characterization and recycling. *Nuclear Measurements, Evaluations and Applications – NEMEA-6. Workshop Proceedings*: 45-50.
16. Pelowitz, D. B. MCNPX User's Manual, Version 2.6.0. 2008. *Report LA-CP-07-1473*. New Mexico, USA: Los Alamos Nat. Lab.
17. Briesmeister, J. F. A General Monte Carlo Code for Neutron and Photon Transport, Version 4B. 1997. *Report LA-12625-M*. New Mexico, USA: Los Alamos Nat. Lab.
18. Garbaras, A.; Andriejauskienė, J.; Barisevičiūtė, R.; Remeikis, V. 2008. Tracing of atmospheric aerosol sources using stable carbon isotopes. *Lith. J. Phys*. 48: 259-264.

19. Gudelis, A.; Gvozdaitė, R.; Lukoševičius, Š. 2009. On determination of radiocarbon leakage from a shallow-land radioactive waste repository. *LSC 2008, Advances in Liquid Scintillation Spectrometry*: 415-420. Tucson, USA: Radiocarbon.
20. Garbaras, A.; Rimšelytė, I.; Kvietkus, K.; Remeikis, V. 2009. $\delta^{13}C$ values in size-segregated atmospheric carbonaceous aerosols at a rural site in Lithuania. *Lith. J. Phys.* 49: 229-236.
21. Poncet, R. 2003. Characterization of Graphite Sleeves From Bugey 1 EDF Plant for Permanent Disposal - Measurement and Calculation of Scaling Factors for Difficult-to-Measure Nuclides. *Proc. of the Waste Management 2003 Symposium*: 23-27. Tucson, USA: WM Symposia.
22. Serapinas, P.; Šalkauskas, J.; Ežerinskis, Ž.; Acus, A. 2010. Local thermodynamic equilibrium modeling of ionization of impurities in argon inductively coupled plasma. *Spectrochimica Acta Part B* 65: 15–23.
23. Ancius, D. 2006. Evolution of the Radionuclide Composition of the RBMK–1500 Reactor Core Graphite. *PhD thesis*. Vilnius, Lithuania: Vilnius University (in Lithuanian).
24. IAEA 2003. Clean laboratories and clean rooms for analysis of radionuclides and trace elements. *Technical Report Series*: 1339. Vienna, Austria: International Atomic Energy Agency.
25. Frolov, V. V.; Kruchkov, A. V.; Kuznecov, J. N.; Moskin, V. A.; Pankratev, J. V.; Romenkov. A. A. 2004. Possibility of burning irradiated graphite from decommissioned nuclear power-generating units. *At. Energ*. 97: 781-784.
26. Takahashi, R.; Toyahara, M.; Maruki, S.; Ueda H. 2001. Investigation of morphology and impurity of nuclear grade graphite and leaching mechanism of Carbon-14. *Nuclear Graphite Waste Management. Proc. of IAEA Technical Committee meeting held in Manchester, U.K, 18-20 October 1999*: 176-190. Vienna, Austria: International Atomic Energy Agency.